Bioinspiration &
Biomimetics

ACCEPTED MANUSCRIPT • OPEN ACCESS

Development of a Bio-robotic Swimmer Based on the Maneuverability of the California Sea Lion

To cite this article before publication: Nicholas Marcouiller *et al* 2026 *Bioinspir. Biomim.* in press https://doi.org/10.1088/1748-3190/ae7788

IOP Publishing *Journal* **Vol** (Year) 000000 WORD TEMPLATE

Bioinspiration & Biomimetics

PAPER

Crossmark

RECEIVED
dd Month Year

REVISED
dd Month Year

ACCEPTED
dd Month Year

PUBLISHED
dd Month Year

Development of a Bio-robotic Swimmer Based on the Maneuverability of the California Sea Lion

Nicholas Marcouiller[1, *], Shraman Kadapa[1], Anthony Drago[1], Frank E. Fish[2], Magan L. Leftwich[3], Harry G. Kwatny[1], and James L. Tangorra[1]

[1] Drexel University
[2] West Chester University
[3] The George Washington University

*Author to whom any correspondence should be addressed.

E-mail: nm875@drexel.edu

Keywords: Maneuverability, Bio-inspired Robotics, California Sea Lion, Multi-body Control Surfaces, Unmanned Underwater Vehicle

Abstract

The development of unmanned underwater vehicles (UUVs) capable of operating in complex environments, such as coastal regions with obstacles and dynamic flows, requires new and effective maneuvering techniques to overcome the limitations of current underwater systems. UUVs that can operate in these zones have broad applications, including environmental monitoring, defense, and infrastructure inspection. By studying the swimming and maneuvering strategies of marine organisms, researchers can develop UUVs that integrate biologically inspired characteristics to enhance performance. The California sea lion (Zalophus californianus) was selected as a biological model due to its swimming and maneuvering capabilities in both the open ocean and through the high-energy surf zone. This paper presents the development and validation of a novel, multi-bodied, bio-robotic system with flipper-based propulsion modeled after the California sea lion. An articulatable head and pelvis, flexible fore flippers that generate 3D forces, and adjustable hind flippers were identified as potential contributors to its mobility, as supported by existing research and video analysis. Through a variety of tests, the system demonstrated its ability to serve as a research platform for systematically evaluating how these features influence swimming and maneuvering. Experimental results demonstrate its ability to use hydrostatic and hydrodynamic forces to move repeatably in 3D space, providing a foundation for assessing the role of body articulation and flipper movements in underwater locomotion.

1. Introduction

Unmanned Underwater Vehicles (UUVs) play a crucial role across a wide array of maritime operations, including scientific research, commercial endeavors, and defense applications; however, their limited maneuverability often restricts their operational reach. While UUVs are increasingly used in the open ocean, there is growing interest in expanding their capabilities to littoral zones, rivers, harbors, and surf zones where maneuverability plays a key role in their success [1], [2]. These missions would frequently require UUVs to navigate tight spaces, avoid obstacles, and execute rapid turns and directional changes in response to turbulent and occluded flow conditions. To operate effectively in these complex, high-energy environments, UUVs would need to be highly maneuverable, requiring further advancements.

Aquatic animals, particularly those adept at navigating high-energy environments, serve as valuable models for enhancing the maneuverability of underwater vehicles. Their remarkable locomotion strategies, which include coordinated body segment movement and adaptive high-speed swimming patterns, enable agile maneuvering in complex, cluttered environments [3]. Studying the morphology, physiology, and kinematics of these biological systems directly informs the development of robotic platforms with improved propulsive efficiency, maneuverability, agility, stability, station holding, and stealth [4]. While significant progress has been made in understanding underwater animal locomotion [5], [6], current underwater systems have yet to fully exploit the characteristics such as body-fin coordination, adaptable compliance, or dynamic vortex manipulation that enable certain aquatic animals to maneuver effectively in diverse flow conditions [7], [8], [9]. Among these, the California sea lion (*Zalophus californianus*) stands out as a prime subject of advanced research [10], [11], [12], [13]. The California sea lion is capable of swimming at 9.7 m/s and diving to a maximum depth of 274 m [14], [15], [16]. Its exceptional ability to navigate complex underwater environments, where it encounters obstacles and energetic flows, makes it an invaluable model for a bio-inspired design [17], [18]. Notably, sea lions have achieved turning rates of up to 690°/s and minimum unpowered (i.e., without active propulsion) turning radii as small as 0.09 body lengths [18]. This high degree of maneuverability can be partly attributed to the animal's coordinated use of its powerful flippers and flexible body [10], [17]. Ultimately, understanding these animals' swimming and maneuvering strategies provides a crucial foundation for applying such techniques in dynamic conditions, offering key insights for developing UUVs capable of operating across varied flow regimes.

The objective of this work was to develop, characterize, and validate a freely swimming bio-robotic research platform modeled after the California sea lion as a system capable of investigating morphological and kinematic traits that contribute to swimming and maneuvering. This platform, named the Stroke Experimentation and Maneuver Optimizing Underwater Robot (SEAMOUR) (Figure 1), was specifically designed to investigate various propulsion and maneuvering techniques through coordinated flipper and body motions. Tests were conducted to explore rectilinear swimming approaches and the use of multiple control surfaces located anterior and posterior of the robot's center of mass to produce pitch and yaw turns. The system's repeatable and versatile functionality makes it ideal for understanding the diverse swimming and maneuvering techniques employed by California sea lions. Studies using the system provide a foundation for identifying design features that can enhance UUV maneuverability, with future work exploring performance in dynamic flow environments.

While traditional UUVs possess varied strengths, their inherent characteristics consistently limit their effectiveness in complex, high-energy environments. For example, torpedo-shaped UUVs that use a single axial propeller operate with limited control surfaces and are designed to prioritize stability and speed for navigating unobstructed open water, an environment where they consistently perform well [19], [20]. While box-frame UUVs can be equipped with a variety of payloads and have multiple propulsors, their large, flat shape generates significant drag at high speeds and can be easily perturbed in energetic environments [21], [22]. Lastly, glider-type UUVs are highly efficient for long-distance travel in open water but have limited speed and agility [23], [24], [25]. As a result, there remains a critical need for systems capable of operating in dynamic coastal environments.

Biomimetic robotics has demonstrated significant success in developing versatile systems that leverage intricate biological traits, offering a powerful alternative to conventional engineering paradigms. While propeller-based systems allow for precise and predictable adjustments to speed and direction through direct control of rotation speed and thrust, animals, in contrast, use intricate movements of their flexible appendages and bodies to generate multidimensional forces [26], [18]. Over the years, numerous researchers have worked on developing systems inspired by marine creatures, including various fish to understand the use of multiple fins for propulsion and maneuvering [27], [28], [29]; sea turtles and cownose rays to explore the potential of soft actuators [30], [31]; and sea snakes/eels to investigate the use of multi-bodied systems [32], [33], to name a few. By incorporating biologically derived characteristics into traditionally shaped UUVs, some researchers have already demonstrated improvements in system maneuverability [34], [35]. The application of biological principles consistently underscores the immense potential of biomimetics, further validating the approach of using highly agile models like the California sea lion to significantly advance UUV maneuverability and performance across diverse environments.

This work focuses on decomposing the morphology and kinematics of the California sea lion to translate these biological features into a robotic system; consequently, the methods detailed herein explain key design decisions, while experimental trials validate the platform's utility for investigating underwater swimming and maneuvering. With that, the remainder of this paper is organized as follows. The methods section includes four sub-sections: the first provides background on the California sea lion and its common locomotory techniques; the second discusses the extraction of flipper and body kinematics; the third describes the design of the bio-robotic system; and the final sub-section outlines the experimental setup and data collection techniques. A combined results and discussion section then validates the platform by examining the design's static stability, the efficacy of various rectilinear swimming approaches, and the system's performance during pitch and yaw maneuvers. Finally, the paper concludes with a summary of key findings and a discussion of future research directions.

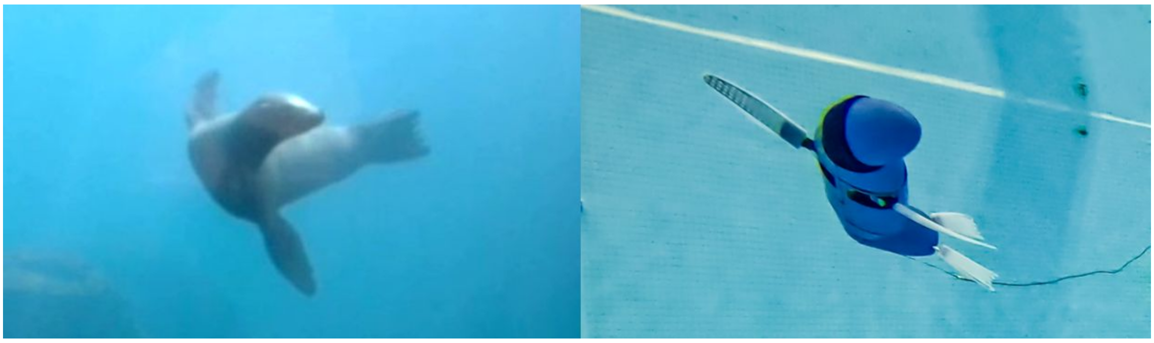

Figure 1. California sea lion and SEAMOUR performing banking turn maneuver

2. Methods

2.1. Background of California Sea Lion Swimming and Maneuvering

The California sea lion (*Zalophus californianus*) was selected as the model organism for this study due to its versatility and exceptional performance in both open ocean and dynamic coastal environments. Sea lions regularly navigate complex habitats including kelp forests, rocky shorelines, and turbulent surf zones, making maneuverability a critical factor in their ecological success [18]. Adult sea lions, which typically measure around 1.81 m in length, exhibit impressive aquatic performance like cruising at sustained speeds of 3.5 m/s [17], executing porpoising leaps of 0.94 m in height and 1.90 m in length at 2 m/s, and performing banking turns with minimum radii of 0.29 m at 3.2 m/s [18], [36]. Their capabilities also extend beyond the water, as they can transition to land and move efficiently using walking or galloping gaits [10], [37]. Sea lions retain mobility in both the fore and hind limbs, providing distinct mechanical strategies for propulsion, stabilization, and maneuvering. In the water, the fore flippers serve as the primary propulsors and control surfaces, while the hind flippers assist with stabilization and maneuvering [18], [36]. Together, these traits make the California sea lion an ideal biological model for investigating aquatic locomotion, offering high maneuverability through coordinated use of its flippers and body across a range of aquatic environments (Figure 2).

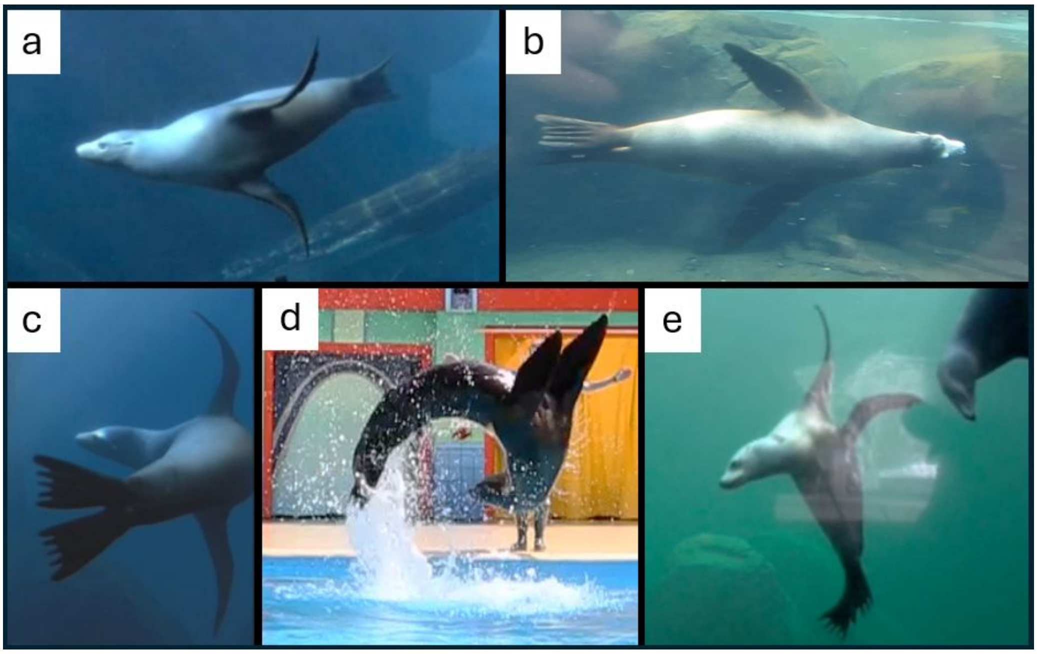

Figure 2. California sea lion during various stages of swimming and maneuvering. (a) Mid propulsive stroke, (b) Gliding, (c) Banking turn, (d) Back flip, (e) Darting to track object

The California sea lion primarily relies on its fore flippers for propulsion during swimming, with minimal contribution from the hind flippers or other body sections. The propulsive stroke has been categorized into three distinct phases: recovery, power, and paddle (Figure 3) [12], defined by the motion at the base of the flipper (shoulder/elbow joints). The recovery phase begins and ends with the fore flippers retracted, medially rotated, and held against the ventrolateral surface of the body. During the recovery phase, the flippers are laterally rotated and abducted, bringing them near a zero angle of attack with the flow. As the flippers are further abducted, they rotate to a positive angle of attack. Lateral rotation slows as medial rotation begins. The power phase starts as medial rotation continues, and the flippers are adducted, resulting in a noticeable dorsal flexion of the distal two-thirds. The flippers' orientation then changes from a positive to a negative angle of attack as they pass the body midline. Rotation slows as adduction continues until the flippers are fully extended beneath the body. At the start of the paddle phase of the stroke, the flippers are maximally adducted and medial rotation continues as they are retracted. The flippers are then forcefully brought upward and inward toward the body [12]. Finally, the flippers return to a streamlined position next to the body [38]. In steady swimming, the hind flippers are typically positioned in an inverted V-shape with little head movement [17] and between strokes the fore flippers may be adducted against the body to create a streamlined profile [36]. Throughout these studies this stroke is referred to as the characteristic stroke and acts as the foundation to other swimming approaches that are explored using the bio-robotic system.

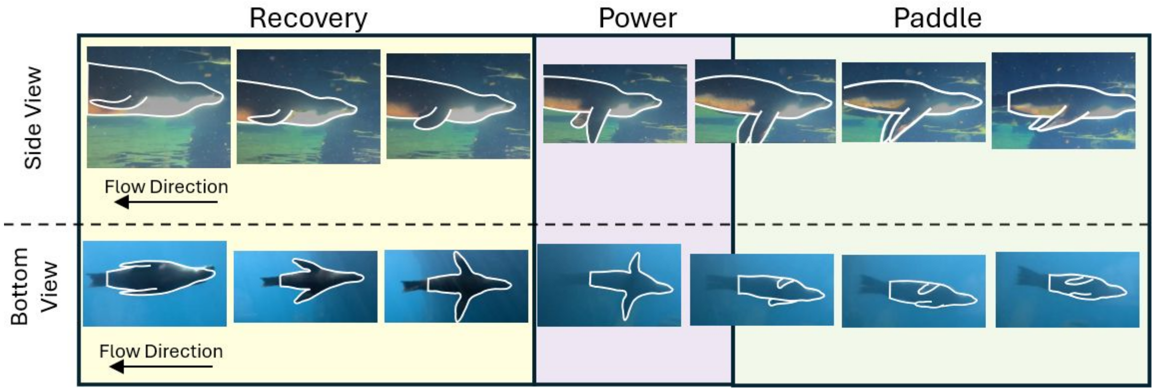

Figure 3. Characteristic stroke recovery, power, and paddle phases from side and bottom views.

The California sea lion employs a variety of strategies to maneuver through the water, with one of the most common being the execution of a banking turn. This maneuver showcases the animal's high maneuverability and highlights the coordinated use of body and flipper movements required to rotate the body about multiple axes. Notably, banking turns enable sharp, unpowered changes in direction, achieving smaller turning radii than powered turns [18], [36]. To initiate a banking turn, the sea lion first rotates its head laterally toward the desired direction of travel. This motion is followed by abduction of the fore flippers and axial body rotation about the longitudinal axis. As the body continues to roll, the hind flippers are angled dorsally into the vertical plane, with an abduction of the digits. Simultaneously, the body undergoes lateral flexion as the head and pelvic region bend toward the center of the turn as the body is bent dorsally producing a continuous, coordinated turn. To complete the turn the animal straightens its body, reducing flexion of the vertebral column and re-aligning with the intended direction of travel. At the same time, the fore flippers are used to accelerate the body out of the turn as the flippers are adducted and retracted to lay appressed against the body. The body then reverses its roll, returning to its starting orientation to resume steady swimming or gliding (Figure 4) [17], [36]. The coordinated body and flipper kinematics demonstrated in this maneuver provide valuable biomechanical principles for informing the design of the robotic system and guiding the development of maneuverability strategies.

Figure 4. California sea lion performing a 90° banking turn. (a) Before the turn, (b) during the turn, (c) coming out of the turn, and (d) after the turn.

2.2 Kinematics of Biological System

To identify the degrees of freedom required for a biorobotic platform, the swimming and maneuvering kinematics of California sea lions were analyzed using videos of both trained and untrained subjects. Footage was captured at the Smithsonian Zoological Park (Washington DC) using a stationary high-definition camera (GC-PX100BU, JVC, Japan) recording at 60 frames per second [13]. The large underwater viewing window allowed for observation over a distance of at least three body lengths as the sea lions swam passively. Additional recordings of trained sea lions performing directed maneuvers were collected at SeaWorld Florida and SLEWTHS at Moss Landing Marine Laboratories [36]. Analysis of these videos lead to the identification of four features for swimming and maneuvering: a manipulable head (cervical), an articulatable pelvis (lumbar), hind flippers capable of acting as control surfaces, and fore flippers that serve both as primary propulsion and control surfaces (Figure 5b). To translate these biological features into robotic specifications, kinematic data was extracted using the two-dimensional digital tracking software Kinovea (Kinovea.org, France). Rotations about different axes were measured for each of the four identified segments by selecting video footage where sea lions swam either parallel or perpendicular to the camera. Since each motion was captured from a single perspective, multiple videos from different angles were used to reconstruct a complete movement profile. The data was then aggregated and averaged to establish a standard motion, providing insight into the degrees of freedom required for each body segment. These findings directly informed the design of the actuators for the robotic platform.

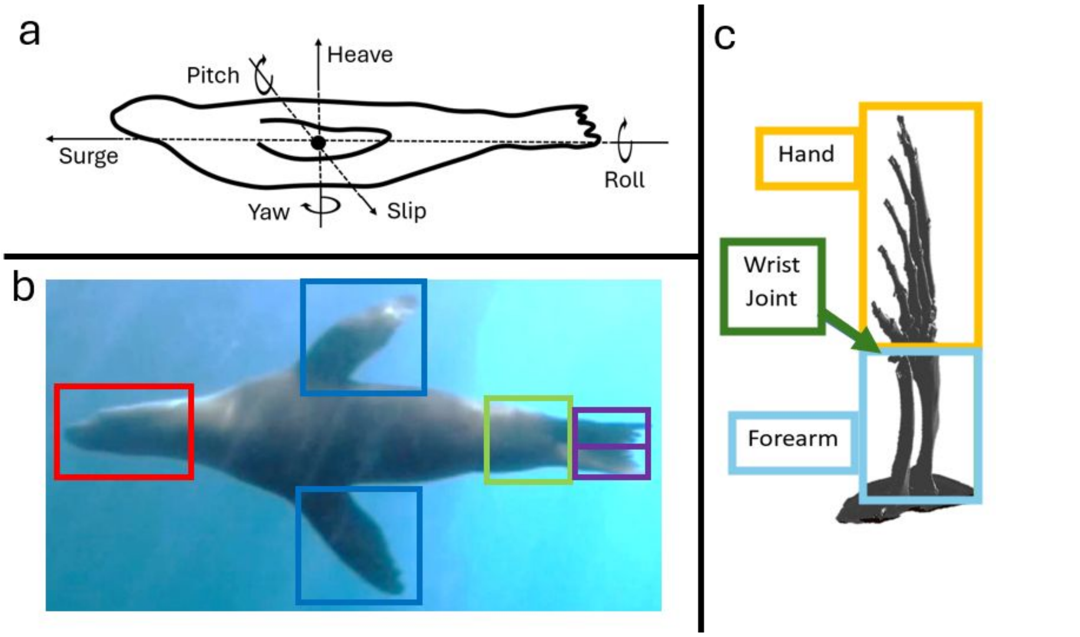

Figure 5. (a) Sea lion body frame of reference. (b) Areas of interest- head (red), fore flippers (blue), pelvis (green), and hind flippers (purple). (c) Sections of sea lion fore flipper bones

To model the 3D kinematics of the fore flipper's motion, an analysis was done that focused on the rotation at the base of the flipper during the characteristic propulsive stroke (Figure 6). The motion was categorized into the three phases, involving $roll_f$, yaw_f, and $pitch_f$ rotations within the flipper's frame of reference (Figure 7). Throughout the stroke, the flippers moved through 140° of $roll_f$, 110° of yaw_f, and 110° of $pitch_f$. The rotations during these motions were plotted, and key inflection points were identified as control points. To validate the stroke analysis, a Piecewise Cubic Hermite Interpolating Polynomial (PCHIP) spline was fitted to various control points, providing a smooth trajectory while ensuring that the fitted motion remained bounded in magnitude. This method allowed for twice-differentiable interpolation, facilitating realistic motion modeling [22]. The fore flipper kinematics were validated using the robotic system to match the motions observed by the animal. This decomposition was not intended to challenge existing descriptions of the fore flipper stroke, but rather to supplement prior findings with a formulation that could be directly implemented on the robotic platform for the present experiments.

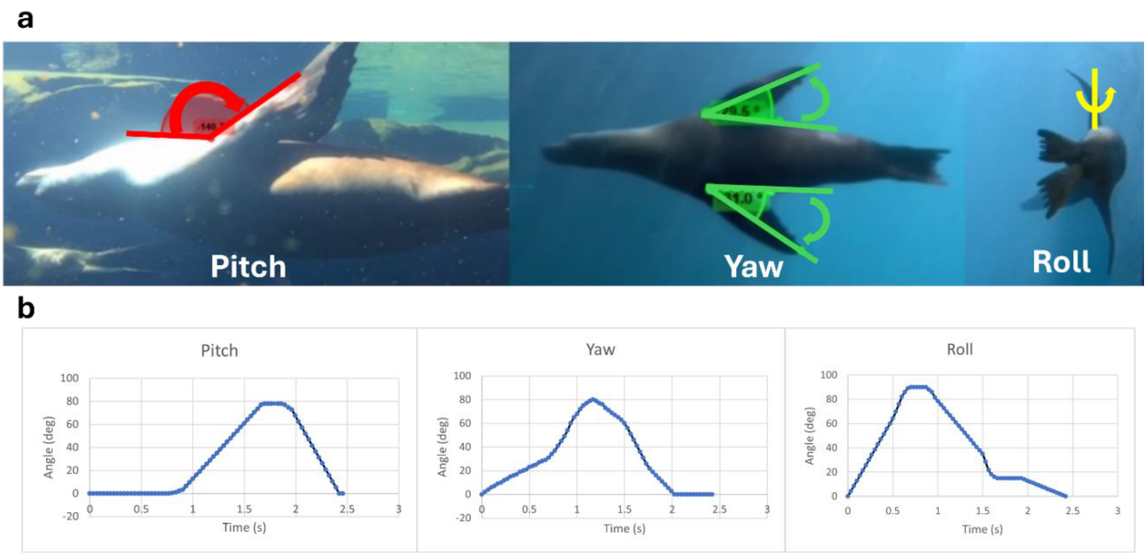

Figure 6. (a) Kinovea tracking software used for decomposition of fore flipper kinematics. Rotations taken in flipper frame. (Left) pitch$_f$, (Center) yaw$_f$, (Right) roll$_f$. (b) Resultant tracking data for the characteristic stroke.

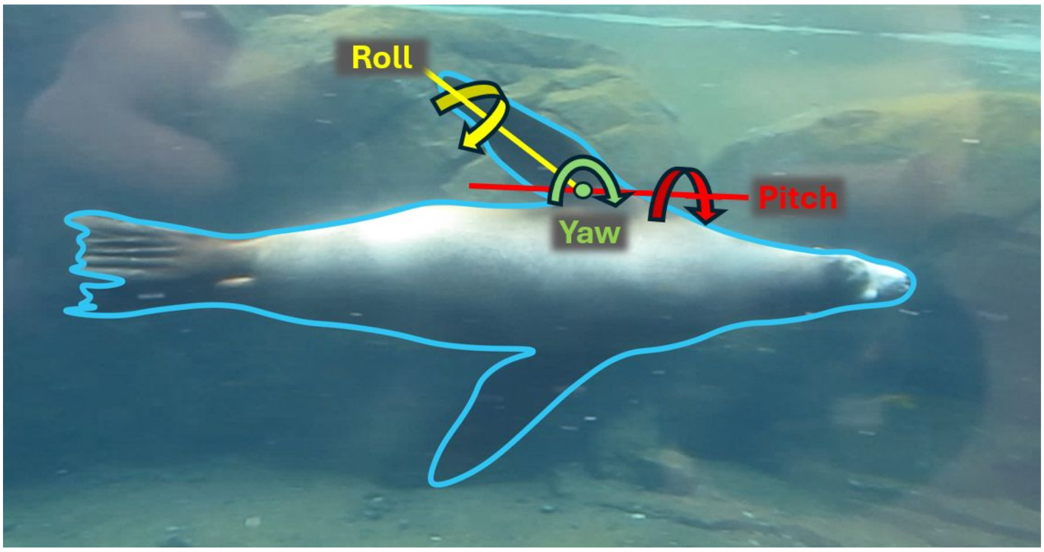

Figure 7. Fore flipper frame of reference. Yellow axis longitudinal through center of flipper represents roll$_f$, green axis perpendicular to flipper at shoulder represents yaw$_f$, red axis parallel to body at shoulder joint represents pitch$_f$.

The bending of the fore flippers was identified as an important factor for propulsion and was therefore analyzed to ensure it could be accurately modeled in the robotic system. Based on the work of Friedman and Leftwich [13], along with additional tracking conducted for this study, it was found that most of the bending occurs at the wrist joint, with continuous flexion extending through the digits (Figure 5c), (Figure 10). The amount of flipper deformation will influence both the direction and magnitude of the propulsive forces they generate. As a result, accurately modeling fore flipper bending will be critical to the development of the bio-robotic system.

The same two-dimensional tracking technique was used to capture the motions of the head, pelvis, and hind flippers during a banking turn. Head motion was tracked from the body to the tip of the nose, while pelvic motion was measured from the body to the base of the tail. During the maneuver, the head was observed to roll a maximum of approximately 90°, yaw 40°, and pitch 90°, while the pelvis rolled 20°, yawed 30°, and pitched 80°. Throughout the turn, the hind flippers yawed 35° and rolled 60° [36]. It remained unclear whether the pitching of the hind flippers resulted from joint articulation or passive flexibility of the flippers. Together, these measurements offered important guidance for modeling the sea lion's turning mechanics in a bio-robotic system.

2.3 Bio-Robotic System Design

2.3.1. Overview

Based on the observations and analyses discussed in the previous sections, the Stroke Experimentation and Maneuver Optimizing Underwater Robot (SEAMOUR) was developed as a versatile research platform to investigate swimming and maneuvering techniques. Its design enabled investigations into various swimming and maneuvering strategies through the actuation of multiple control surfaces, including the head, fore flippers, pelvis, and hind flippers (Figure 8). SEAMOUR was designed with features to proportionally match those of a sea lion, with a total length of 1.3m. The system features 14 actively controlled degrees of freedom (DoF), powered by high-torque waterproof servo motors (WR-7701, Xpert RC, USA). These include ±60° of pitch and yaw at both the head and pelvis joints, 160° of roll$_f$, 110° of yaw$_f$, and 130° of pitch$_f$ at the fore flippers, and ±30° of yaw with 160° of roll at the hind flippers. This arrangement was selected to enable precise, repeatable, and independently controllable motions, providing a highly adjustable platform capable of delivering consistent performance across a broad range of swimming and maneuvering experiments.

SEAMOUR was developed as a modular research platform capable of producing biologically relevant motions while supporting a wide range of experimental configurations. To model sea lion body bending the head joint provides independent pitch and yaw actuation for modeling cervical bending, while the pelvic section uses the same mechanism to model lumbar motion. Each degree of freedom features independently adjustable actuation speeds and customizable motion profiles, allowing precise control of joint kinematics. The system's modular design accommodates interchangeable fore flippers with adjustable shape and flexibility, along with interchangeable head shapes and tunable inertial properties. This adaptability allows SEAMOUR to evolve with new hypotheses and experimental needs without requiring a complete system redesign. The platform was engineered for reliable operation in both constrained and unconstrained testing environments, producing repeatable motions for controlled experimentation. Additionally, onboard sensing records the system rotations, enabling analysis of how the robot's kinematics influence its body's movement through the water.

Certain design simplifications were made to prioritize the features being investigated in these initial studies. Continuous body bending in the thoracic section, biologically accurate head shape, and exact flipper scaling and contour were excluded from this iteration of the design to focus on isolating the effects of the included features. Although these other features likely influence swimming performance, their omission allowed for a more controlled evaluation of the targeted kinematic variables. Future work will examine the influence of additional joints, body flexibility, and alternative control surface geometries on swimming and maneuvering performance.

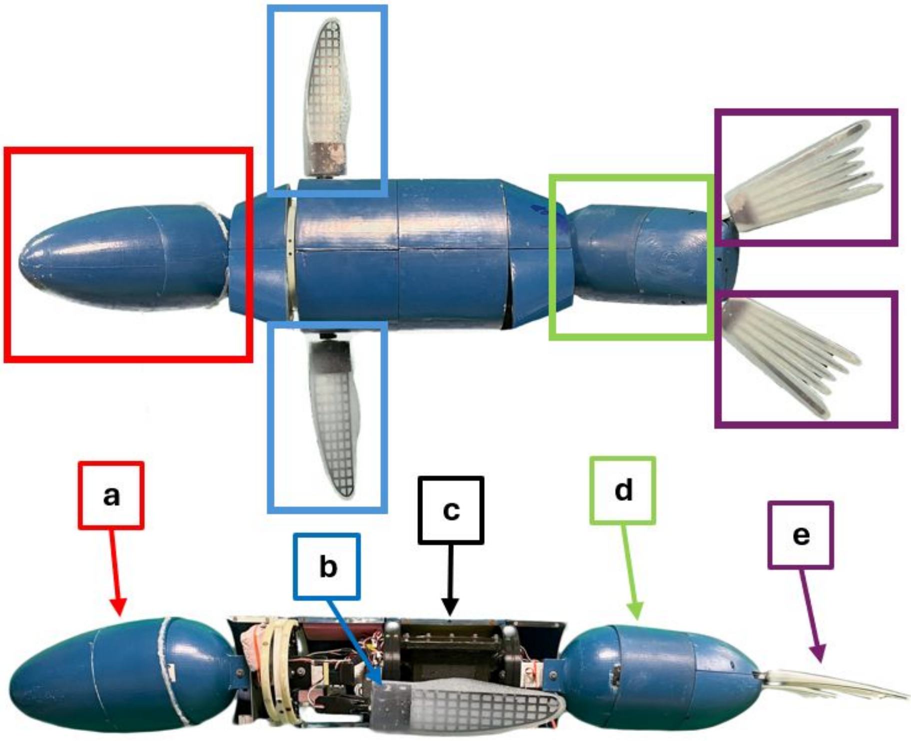

Figure 8. Top: SEAMOUR with head pitched 60°, fore flippers yawed$_f$ and rolled$_f$ 90°, pelvis pitched 60°, hind flippers yawed 25° and rolled 0°. Bottom: SEAMOUR in streamlined position. (a) Head- pitch and yaw DOF, (b) fore flipper motor configuration- roll$_f$, yaw$_f$, and pitch$_f$ DOF, (c) waterproof power and electronics box, (d) Pelvis- pitch and yaw DOF, and (e) hind flippers- yaw and roll DOF.

2.3.2. Main Body

The main body of the robotic platform, representing the thoracic region of the animal, and was designed to enclose all mechanical and computational components within a streamlined ellipsoid shape, closely resembling that of a sea lion [11]. Unlike the animal, this section was made rigid, therefore limiting body bending. SEAMOUR's main body is divided into two sections: the anterior section, which provides mounting for the head and fore flippers, and the posterior section, which contains a waterproof box housing the electronics and provides a mounting point for the pelvic section.

A Raspberry Pi 4B (RPI) provided computational power and broad hardware compatibility, supporting motor control, sensor integration, and remote operation. A PWM-based daughter board (PN 2327, Adafruit, USA) was used for precise servo motor control, while a 9-DOF inertial measurement unit (IMU) (BNO085, PN 4754, Adafruit, USA) captured rotational and acceleration rates (Figure 21). To enable remote operation, the RPI's Wi-Fi antenna was modified so that it could be extended via a cable that breached the water's surface. This antenna could either be dragged behind the robot using a surface float for continuous communication or remain attached to the outer shell after motor trajectories were loaded near the surface reducing drag and eliminating entanglement [39]. The system was also designed with flexibility for future sensor integration, such as a depth sensor for active buoyancy control, a doppler velocity log for precise velocity and position measurements, or pressure sensors for local flow detection.

As the interior of the robot is flooded to enable the modular design, all electrical components were housed within a waterproof box located in the posterior section of the robot. The electronic housing was fabricated in house and allowed SEAMOUR to operate at depths up to 4m. Additional details on the fabrication of the waterproof housing and a schematic for the wiring which details the power distribution and control systems can be found in the Appendix.

2.3.3. Fore Flippers

The fore flippers were designed to model the fundamental motions and bending of the biological sea lion flippers during characteristic swimming and turning maneuvers. Their motion was modeled at the elbow joint of the animal and actuated using three servo motors per flipper, providing independent control of $pitch_f$, yaw_f, and $roll_f$. Described in the fore flipper frame of reference, the $pitch_f$ motor attached the center support structure, next in the chain was the yaw_f motor, and lastly the $roll_f$ motor which acted as the final connection point for the fore flipper (9). To increase the rigidity of the assembly, bearings were added on axis to the $pitch_f$ and $roll_f$ motors to support the radial loads. This assembly accommodates flippers of varying sizes and degrees of flexibility, while the available DoF enables a wide range of motions, ensuring the system is not limited to strictly biologically derived movements. For example, rigid flippers were used in place of the standard flexible flippers during the experimental trials conducted to validate the numerical model of the system [40].

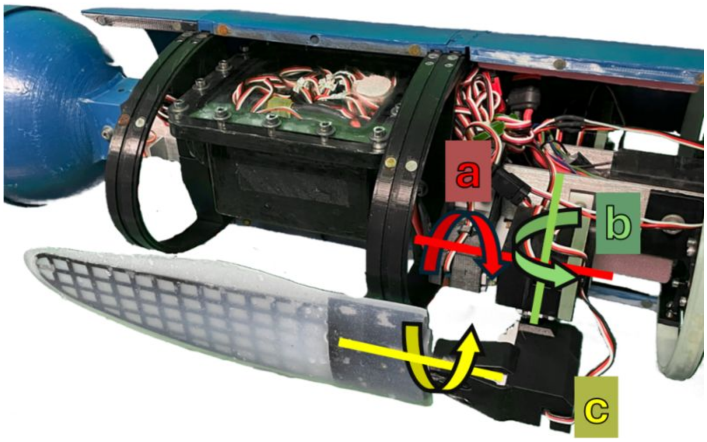

Figure 9. Fore flipper motor assembly. (a) $Pitch_f$ motor. (b) Yaw_f motor. (c) $Roll_f$ motor.

SEAMOUR's fore flippers were designed to model the general shape, proportions, and placement on the body. Certain biological characteristics, such as the trailing edge crenelations [26] and the specific hydrofoil shape [12] were simplified in the robotic system as these features were not the focus of these studies. The fore flippers were positioned to reflect the natural anatomy of a sea lion, but their size was reduced by 17% relative to a proportional scale to accommodate motor torque and speed limitations while maintaining key functional trends associated with propulsion and maneuvering. Tests showed that the hydrodynamic lift generated by the modeled fore flippers were similar to the actual sea lion fore flipper over a range of angles of attacks; see the supplementary document for additional details.

The bending of the fore flippers was modeled based on the bending profile observed during the characteristic stroke. Each flipper was designed with a rigid base and a gridded support structure that enabled both span-wise and chord-wise bending to be modified during the design process (**Error! Reference source not found.**). The proportions of the rigid and flexible sections were derived from the animal's anatomy, where the forearm represented two-fifths and the hand portion represented three-fifths of the flipper (Figure 5B) [12]. This design ensured the fabricated flippers modeled natural bending from the wrist joint through the finger-like structure [10], [13]. Bending of the fore flipper was passively induced by self-loading during movement through water, where the amount of bending could be adjusted by modifying the taper of the grid pattern or the number of grid sections. Finite element analysis (FEA), conducted using SolidWorks CAD software (SolidWorks, USA), was employed to evaluate the structural response of the bio-robotic flipper. To accurately model the hydrodynamic loading during the characteristic stroke, a non-uniform, parabolic pressure distribution was applied to the flipper surface. The intensity of this distribution was derived from the maximum angular velocity of the motors

(0.14 s/60°, or approximately ω= 7.48 rad/s), representing the peak operational load. The loading was defined by the equation

$$P(r) = \frac{1}{2}\rho C_d(\omega r)^2 = 0.0308 * r^2 \quad (1)$$

where P is pressure in Pa, r is the distance from the pivot in mm, ρ density of water, and C_d is the coefficient of drag for a flat plate. A nonlinear solver was utilized to account for large displacements and geometric stiffening resulting from the high flexibility of the lattice-reinforced flipper structure (Figure 10). This simulation facilitated fine-tuning of the flipper's structure before fabrication and validation on the mechanical system. The analysis predicted a tip displacement of 0.108 m, which when scaled closely matched the bending characteristics observed in the biological system.

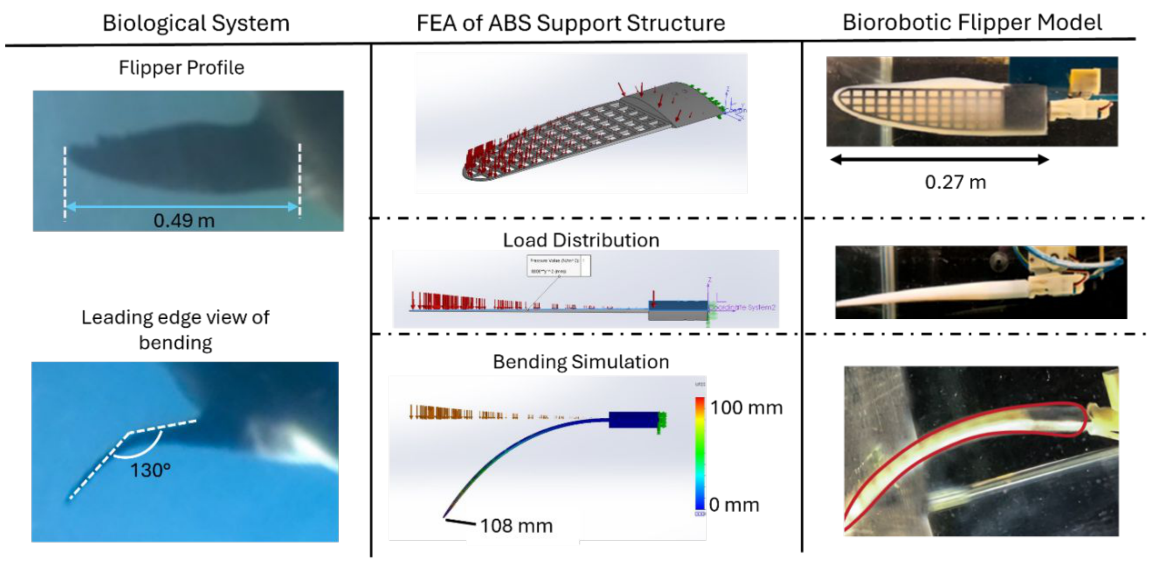

Figure 10. Evaluation and validation of fore flipper design. Left: Biological flipper shape and bending. Center: Fore flipper support structure during FEA. Right: Fabricated silicone cased fore flipper during experimental bending validation.

The fore flippers were fabricated using a multi-step casting process (**Error! Reference source not found.**). First a positive cast was made to form the negative mold. After positioning the gridded support structure in the mold, a two-part silicone with a shore hardness of 30A (Dragon Skin 30, Smooth-On, USA) was used to cast the flippers. See the Appendix for additional details on this process.

2.3.4. Pelvis

The pelvic section was designed to emulate the bending of the animal's lumbar region using a two-axis gimbal mechanism driven by two motors. This setup provides independent control over pitch and yaw movements. The gimbal is enclosed within a half-dome structure, with its axes aligned to a shared center of curvature, allowing up to ±60° of articulation from the midline in each direction (Figure 13b). As minimal pelvic roll rotation was observed by the animal, rotation about this axis was excluded from the joint design. The pelvic section also integrates the motors responsible for hind flipper actuation and voids throughout the section were used for ballast material.

2.3.5. Head

SEAMOUR's head was mounted on a two-axis gimbal system, modeling the degrees of freedom of a sea lion's cervical region. In these initial studies, the head was axisymmetric to reduce mechanical complexity, measuring 0.265 m in length with a cross-sectional area of 0.02 m^2. To minimize drag and mitigate potential flow disruptions caused by head articulation, a four-way stretch spandex fabric was secured between the head and the tapered body shell (Figure 11a). The head mounting system was designed for interchangeable head shapes and sizes, allowing for future investigations into the effects of head asymmetry. Beyond its adaptable form, the head also accommodated ballast material and space for a future vision system.

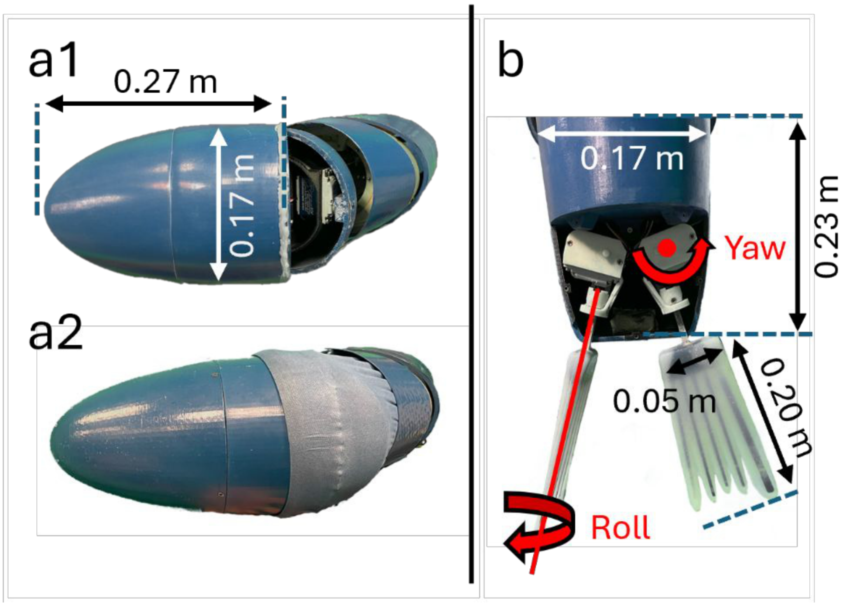

Figure 11. Head yawed 60° without (a1) and with (a2) four-way stretch fabric. (b) Pelvic section with exposed hind flipper yaw and roll motors.

2.3.6. Hind Flippers

The hind flippers of the bio-robotic system were designed to model the kinematics of the animal using flexible flippers that could yaw and roll independently. Housed within the pelvic section, the hind flipper motors enable each flipper to yaw a maximum of ±30° from midline and roll 160° (Figure 11B). The flexible flippers were fabricated in the same manner as the fore flippers; however, their bending characteristics were not explicitly characterized, as the influence of their flexibility was not explored during these studies. When comparing the modeled hind flippers to the actual animal the hydrodynamic lift generated over a range of angles of attacks were similar; see the supplementary document for additional details.

2.3.7. Trim

Lead weights and extruded polystyrene foam were added to designated voids in the head, body, and pelvis to adjust the locations of the center of gravity (CoG) and center of buoyancy (CoB), achieving neutral buoyancy and a horizontal equilibrium in the water. These adjustments positioned the CoB above the CoG in both the x-z and y-z planes (Figure 12A), creating moments that affected the system's roll and pitch stability [41]. The head, body, and pelvis sections were individually trimmed for neutral buoyancy before being assembled. Trim modifications were also used to shift the CoG and CoB of the overall system anteriorly or posteriorly, with efforts made to align their positions close to the fore flippers as seen in the biological model [18]. Each one of these adjustments were updated in the 3D CAD model of SEAMOUR (Creo Parametric 10.0, USA), which was then used to calculate the CoG of the system. In the final configuration, the CoG for the entire system was calculated to be -0.07 m in the x-direction from the coordinate frame (Figure 12B), which places it 0.12 m in front of the system's overall center.

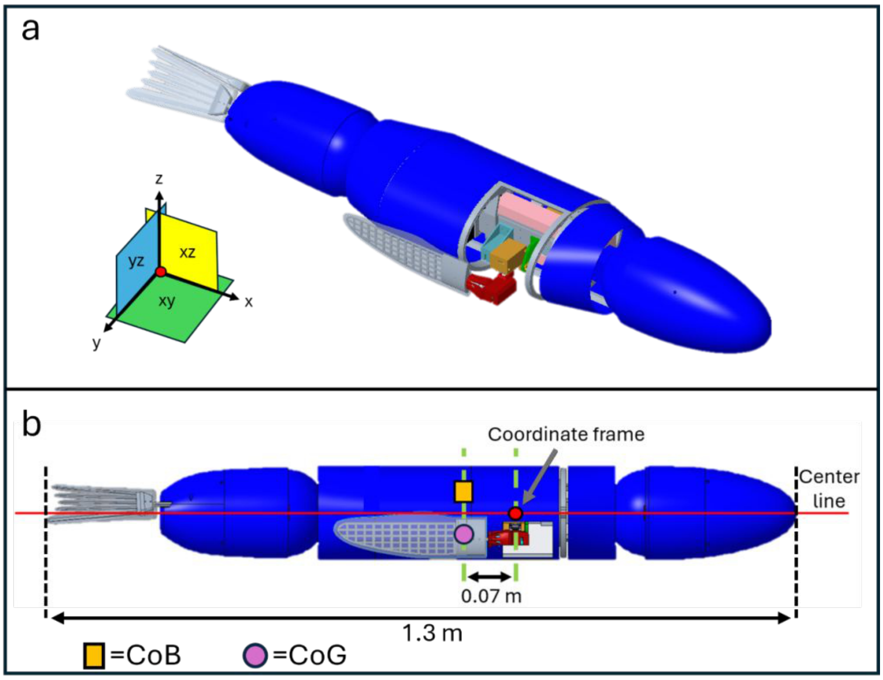

Figure 12. (a) SEAMOUR body frame of reference plane and axis in CAD. (b) Center of gravity (purple circle) and center of buoyancy region (orange box) for the entire system

To calculate the CoB, the solid parts and any air pockets in the CAD model needed to be set to a uniform density. Making these adjustments would allow the CoG calculator in the 3D CAD software to be used to find the centroid of the displaced volume of fluid (i.e. CoB). This calculation showed that the CoB was also located -0.07 m in the x-direction from the coordinate frame.

2.4. Experimental Procedure and Data Collection

2.4.1. Overview

Experiments were conducted to evaluate the design of the system and its utility as a research platform by executing various swimming and maneuvering tests. These tests were designed to characterize the system's dynamics, assess the use of various control surfaces, and identify performance trends as the robot moved freely through the water. Prior to testing, the system was trimmed to be horizontally level, with individual body sections trimmed for neutral buoyancy. The first set of experiments examined how the systems current CoG and CoB influenced its ability to return to equilibrium after being displaced at various angles (N=120), with stability assessed by measuring the response and settling times as the body realigned. The second set of experiments evaluated how different combinations of fore flipper and body motions could be used to achieve straight line swimming (N=15), with body orientation and x- and z-axis translations recorded to assess each stroke's ability to maintain a straight and level trajectories. The third set of trials investigated the use of head and pelvis motions to perform repeatable pitch and yaw maneuvers (N=60), which were assessed by recording body orientation to quantifying angular positions and rates as control surfaces were actuated through a range of angles. Collectively these tests were conducted to evaluate the systems response and explore its utility as an experimental platform.

2.4.2. Passive Roll and Pitch Stability

The impact of the system's CoG and CoB locations on its roll and pitch stability were determined by observing the body's angular rate as it returned to equilibrium. Experiments were conducted by manually positioning the robot at various roll and pitch angles before releasing it. An onboard IMU recorded the resulting angular changes over time at a sampling rate of 20 Hz (Figure 13). Tests were conducted with roll and pitch angles of 20°, 40°, 60°, and 80°. Pitch tests were performed with the system in a streamlined position, with the fore flippers held against the body. Roll tests were conducted under two conditions: with the fore flippers streamlined and with the fore flippers extended ($yawed_f$ and $rolled_f$ 90°). The robot was tested by rolling it to the left and right, as well as pitching it in head-up and pelvic-up orientations. The data was offset to align t=0 with the release time and trimmed to 16 seconds. The systems pitch or roll orientation from three trials were averaged for analysis. The standard error between trials was calculated and was represented by the shaded region on the plots.

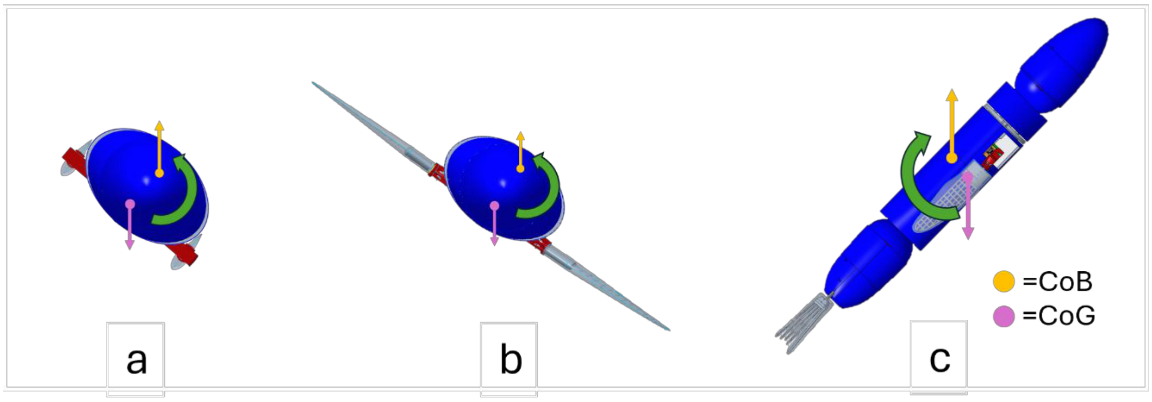

Figure 13. Body orientation for each static stability test. Orange arrow indicates force from CoB and purple arrow is force from CoG. Rotation due to restoring moment depicted by direction of green arrow. (a) Roll test with fore flippers in streamlined position. (b) Roll test with fore flippers in extended position ($yawed_f$ 90° and $rolled_f$ 90°). (c) Pitch test with fore flippers in streamlined position.

Settling time was identified as the first instance when the signal entered and remained within a defined threshold band around the final value. This final value was estimated by fitting a linear trend line to the last 7 seconds of the roll data and extrapolating to the endpoint. The threshold band was set as ±0.1° from the final value, allowing for small fluctuations while capturing the signal's convergence behavior. The algorithm checked for continuous periods within this band that lasted for a minimum duration of 0.10 seconds to confirm stability. The first point at which the data satisfied these criteria was recorded as the settling time.

Due to the differences in the data set, a different methodology for calculating the settling time for pitch tests was needed. First the average of the final 10 data points of each test was calculated to represent the steady-state value. A ±0.1° band was established around this steady-state value to define the acceptable range for settling. The settling time was identified as the first time point where the data enters this band and remains within it for the rest of the duration. This approach ensures that the system is considered settled only when it consistently stays close to its final value. These two approaches for determining settling time were necessary because SEAMOUR could not be precisely trimmed to achieve equilibrium at 0° in both the x and y axes.

2.4.3. Straight Line Swimming

Tests were conducted to evaluate the system's ability to create forces to produce straight line swimming using the flipper and body. Three swimming techniques were tested for their effectiveness in producing straight and level translation through the water: a biologically derived characteristic stroke, implemented both with and without the use of the pelvis, and a modified side paddle stroke (Figure 14). Evaluating the system's ability to perform a variety of propulsive gaits is detrimental to the utility of the system to further explore maneuvering techniques.

The kinematics for the characteristic stroke were derived from existing literature and in-house kinematic investigations. This work lead to the development of stroke kinematics based on the animals characteristic stroke that minimized lift and produced optimal thrust [42]. Trials were also conducted where additional control surfaces were articulated during the characteristics stroke to improve the trajectory of system. These tests pitched the pelvic section downward by 15° during the stroke transition (between the power and paddle phases) and gradually returning it to a streamlined position during the recovery phase.

The modified side paddle stroke was designed to utilize only the fore flippers for rectilinear swimming. By manually adjusting the PCHIP spline control points for fore flipper motion, a new swimming gait was developed. This gait was adapted from the best-performing reinforcement-learned gait evaluated in earlier work [43], with slight tuning to accommodate design modifications. This modified stroke replaces the power phase with a side-body paddle motion, allowing control of vertical body movement through flipper roll and pitch adjustments.

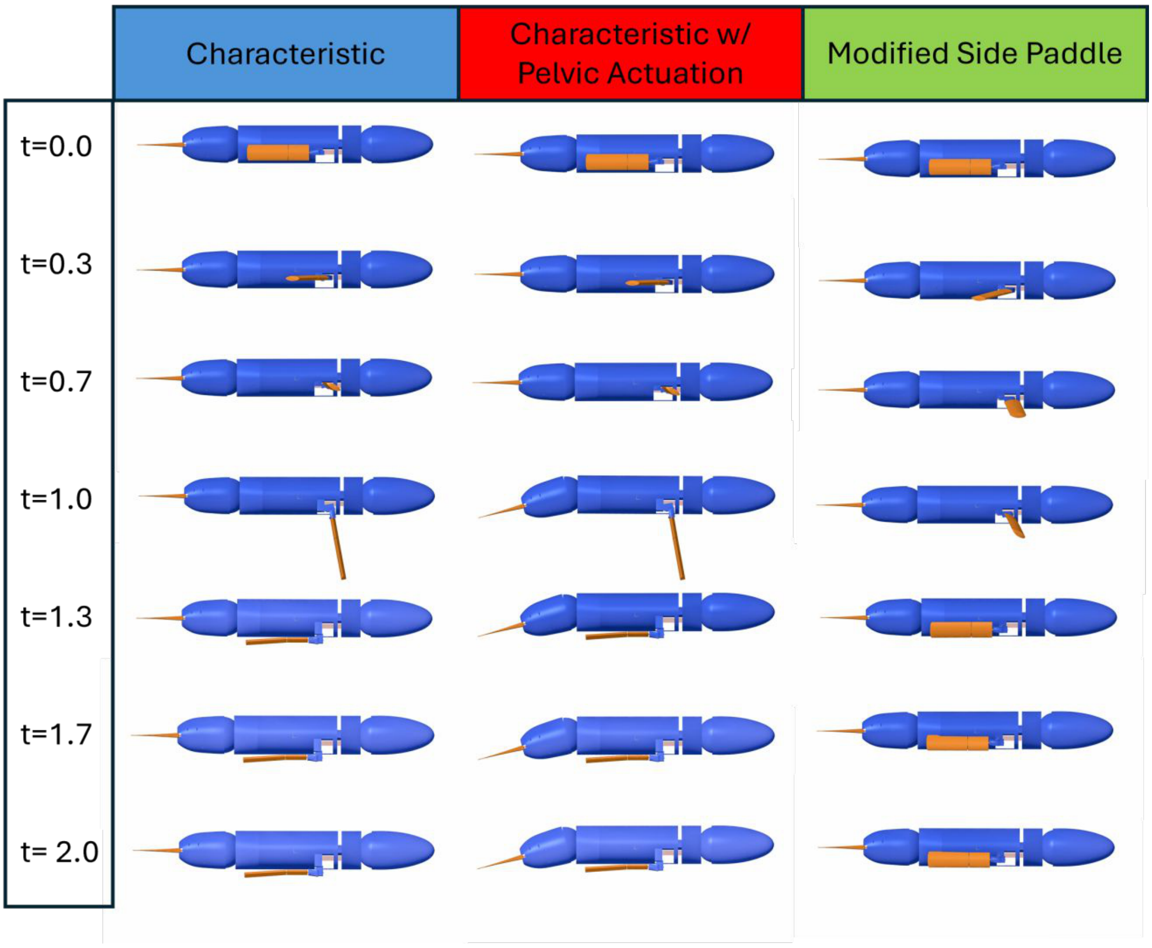

Figure 14. Time sequence from t = 0 to t = 2 seconds showing the three swimming techniques implemented, represented with a CAD model. The final second of each stroke, corresponding to the recovery phase when the flippers reset for the next stroke, is omitted to better highlight the propulsive phases.

During each experiment, the position of SEAMOUR was tracked using a stationary underwater camera while orientation was recorded using an on board IMU. Each stroke type had a three second period with each trial consisting of four consecutive strokes. A GoPro Hero 11 camera (GoPro, USA), positioned to capture the side of the robot as it moved through the water, was set 8 m away and to record at 24 frames per second in 4K resolution using a wide frame of view. The video footage was then post-processed to correct lens distortion, lighting, and color (Adobe Premiere Pro, USA) before being tracked in Kinovea. To calibrate the scale of the video frame, a known length on SEAMOUR was set using the software. Pitch orientation data was collected during each trial using the IMU, which recorded at 20 Hz. The data was recorded two seconds before each trial and continuing throughout the trial; with the initial reading used to correct for any offset in the robot's starting orientation. The position and orientation data from each study were aligned and results averaged across three trials. The variability between the trials calculated as standard error which was represented by the shaded region on each plot.

The system was designed so tests could be run while swimming freely or while attached to a float. Unconstrained tests were conducted utilizing an underwater docking station. This dock positioned the robot at a depth of 0.8 meters and featured two curved supports that matched the contour of the main body's shell. Magnets embedded in a release rod connected to a steel bar running along the length of the posterior shell which allowed the system to be released remotely from the surface. This approach was used during both swimming and maneuvering tests conducted in this paper, which ensured a consistent starting position and orientation for each trial (Figure 15). For constrained testing, the system was designed to be attached to a surface float, restricting its motion to the xy plane while preserving x axis rotations. To accomplish this a Ø160mm FDM 3D-printed Delrin roller bearing was fabricated and positioned between the front taper and main body shells. By attaching the system to a float, its position and orientation can be tracked at the surface and a surface docking system can be implemented for repeatable trials. This approach was not used in the studies presented in this paper, but its utility will be important for future studies.

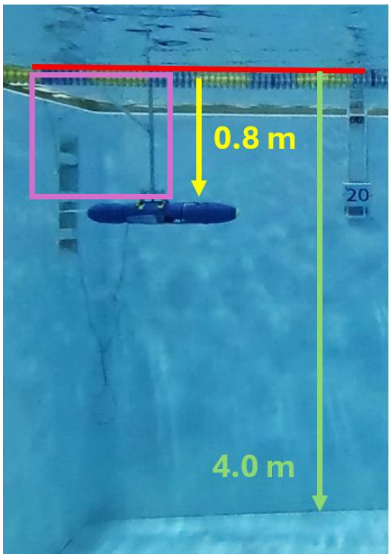

Figure 15. SEAMOUR mounted on unconstrained docking system (purple box) for straight swimming and maneuvering experiments.

2.4.4. Yaw and Pitch Turns

Unconstrained maneuvering trials were conducted to validate the system's ability to generate repeatable 3D trajectories through precise head and pelvic actuation. By testing at both 30° and the 60° maximum actuation limits, these experiments characterize the sensitivity of the platform's turning rates and angular positions to specific joint inputs. During these tests, SEAMOUR swam unconstrained, using its fore flippers to reach an initial velocity of 0.31 m/s at the start of each trial. Following this, the head, pelvis, or both were actuated to either 30° or 60° in yaw or pitch. These pitch and yaw turns were performed unpowered, where additional propulsion did not aid the turn. During the combined tests, the head and pelvic were actuated symmetrically, i.e. head at 30° pitch and pelvic at 30° pitch. Pitch and yaw tests were performed about their respective axes—pitch about the y-axis and yaw about the z-axis. Each actuation was held for 5 seconds, and the IMU recorded the system's orientation. A representative data set of three trials was then averaged, with the standard error between trials calculated to characterize inter-trial variability throughout the turn duration. To provide rigorous statistical support for performance comparisons, additional analyses were performed on the final angular positions and mean turning rates. A One-way Analysis of Variance (ANOVA) was used to determine the statistical significance of joint configuration (head-only, pelvis-only, and combined) on turning performance. Independent t-tests were employed to evaluate the sensitivity of the platform to different actuation angles (30° vs. 60°) and to compare effectiveness between turn axes (pitch vs. yaw). Statistical significance for all tests was defined at $p < 0.05$, and 95% confidence intervals were calculated to assess the reliability of the research platform using a t-distribution with 2 degrees of freedom to assess the reliability of the mean performance. During each actuation, the fore flippers remained in a streamlined position alongside the body, and the hind flippers were held at a roll angle of 0°.

3. Results and Discussion

3.1. Overview

SEAMOUR was successfully developed as a research platform to investigate the use of various biological and non-biological swimming and maneuvering approaches. Across all experimental trials, the system demonstrated consistent, repeatable performance with low positional and angular standard errors, validating SEAMOUR's reliability and versatility as a modular, multi-bodied robotic platform. Initial static stability tests established a baseline, revealing that roll response varied with fore flipper configuration, as extended flippers improved stability by reducing angular velocity, settling time, and overshoot, while pitch maneuvers exhibited lower angular velocities but comparable settling times to roll tests with streamlined flippers. When implementing a biologically derived swimming stroke (characteristic stroke) the system saw significant translation in heave and high pitch changes through the trials. When the pelvis was incorporated during the characteristic stroke, heave translation was mitigated, due to reduced pitching, and surge translation was greatly improved. Further refinement using a modified side paddle stroke eliminated the need for pelvic actuation while still achieving effective forward translation and maintaining a low body pitch angle. In maneuvering trials, the pelvic section had the greatest influence during pitch and yaw maneuvers, while combining head and pelvic articulation saw slight improvements. Overall, pitch-based maneuvers consistently outperformed yaw-based maneuvers under all test conditions. These findings collectively highlight the ability to implement various swimming and maneuvering gaits, which would pave the way for additional gait strategies tailored to specific locomotory objectives.

3.2. Influence of CoG and CoB

As SEAMOUR is a multi-bodied robot, the buoyancy characteristics of its head and pelvic sections can influence the performance of the overall system when articulated. If these independent sections were negatively buoyant, while the overall system was neutrally buoyant, any displacement of these sections from the body's midline would have caused the CoG to shift more than the CoB, causing the system to roll. To mitigate this action, the head and pelvis sections were individually trimmed for neutral buoyancy to minimize the influence of hydrostatic forces, particularly during the maneuverability studies. This configuration ensures that the CoG and CoB shift in unison when individual body sections are articulated.

The CoG, CoB, and moments of inertia are closely interconnected, and their combined configuration significantly affects the maneuverability of the bio-robotic platform. In a configuration where the head and pelvic sections are negatively buoyant while the overall system remains neutrally buoyant, the moments of inertia about the y and z axes will be greater compared to a configuration where each section was independently neutrally buoyant. The former configuration resembled a dumbbell, while the latter was akin to a pipe. Consequently, a negatively buoyant head and pelvis increase the system's pitch and yaw stability, making it suitable for applications prioritizing stable straight swimming. However, this setup is less optimal for a maneuverable system, further justifying the trimming of the CoG/CoB to enhance maneuverability. Understanding and optimizing the moments of inertia are essential in the design of effective underwater vehicles, as the offset and relative positions of the CoG and CoB directly influence a system's stability and the ability to roll, yaw, and pitch. These parameters can be strategically adjusted to achieve specific performance characteristics depending on the operational goals of the vehicle.

3.3. Passive Roll and Pitch Stability

During tests when the system was rolled away from equilibrium, its response varied significantly based on the fore flipper configuration but demonstrated consistent trends across different initial roll angles (Figure 16). Larger initial roll angles resulted in greater overshoot magnitudes when the fore flippers were streamlined, whereas the opposite occurred when the fore flippers were extended. By extending the fore flippers, the angular velocity during the first second is decreased by 66% across all four angles (Table 1). The mean standard error across both roll configurations ranged from ±0.17° to ±0.47° across each 16 second trial (Table 2), demonstrating consistent performance.

With the fore flippers in the streamlined configuration, the roll angle underwent multiple cycles of damped oscillations before settling, while in the extended configuration, stability was achieved after a single damped oscillation. The settling time in Figure 16A and B is denoted by a black dot on each line. This variation in the system's response can be attributed to the difference in drag between configurations. Notably, when comparing the two roll configurations, the settling time was significantly reduced when the fore flippers were extended (abducted). Comparing the streamlined and extended positions revealed that extending the fore flippers reduced settling time by 53% for 40°, 53% for 60°, and 49% for 80° initial roll angles. These tests also show that the settling time was not dependent on the initial release angle.

With the fore flippers extended during the roll test the settling time for release angles of 40°, 60°, and 80° consistently fell between six and seven seconds, while the 20° release angle deviated from this pattern. This was likely due to the system's low restoring moment at smaller initial angles, causing it to settle slightly off the target position after the first overshoot. Consequently, the extrapolated trend line predicted a final value that was farther from the expected position at 15.3s

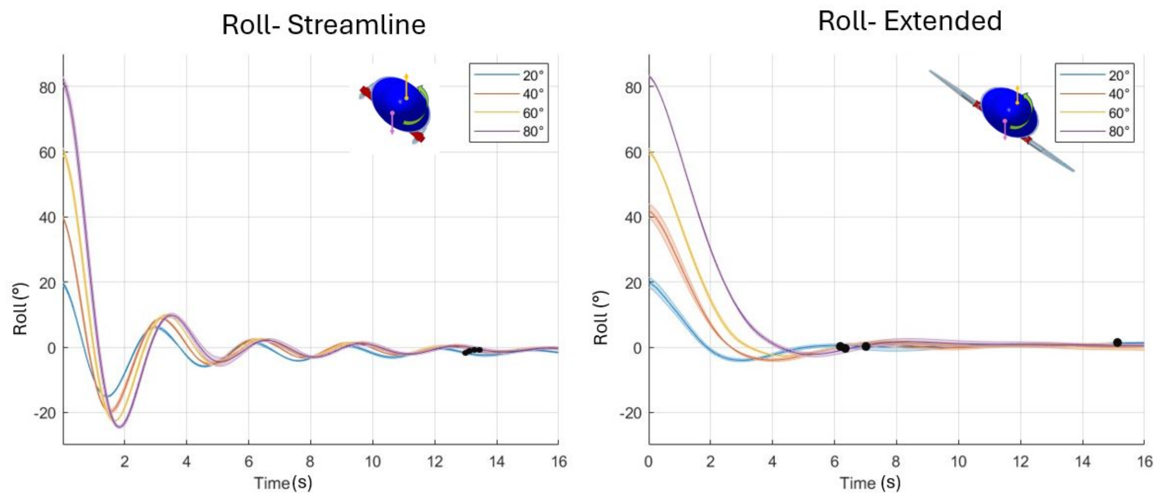

Figure 16. Roll stability plots for initial angles of 20°, 40°, 60°, and 80°. The black dot on each line represents the settling time. (a) time response with fore flippers streamlined next to body and (b) time response for flippers yawed$_f$ and rolled$_f$ 90°.

Table 1. Mean angular velocity during the first second of each trial for fore flipper streamlined and extended configurations at 20°, 40°, 60°, and 80° roll angles from equilibrium.

Mean angular velocity

Fore Flipper Configuration	20° *(°/s)*	40° *(°/s)*	60° *(°/s)*	80° *(°/s)*
Streamline	30	49	61	70
Extended	10	16	22	24

Table 2. Mean standard error for fore flipper streamlined and extended configurations at 20°, 40°, 60°, and 80° roll from equilibrium.

Mean standard error				
Fore Flipper Configuration	20° *(±°)*	40° *(±°)*	60° *(±°)*	80° *(±°)*
Streamline	0.18	0.17	0.22	0.47
Extended	0.33	0.42	0.24	0.35

When the robot was pitched away from its equilibrium and released, it had lower mean angular velocities compared to both roll tests (Table 3), but had comparable settling times to the roll configuration with the flippers in the streamlined position (Figure 17). The increase in drag and moment of inertia during pitch tests resulted in lower angular velocities, preventing the system from overshooting its final value in this orientation. Over the 16 second trials the mean standard error ranged from ±0.66° to ±1.26° (Table 4).

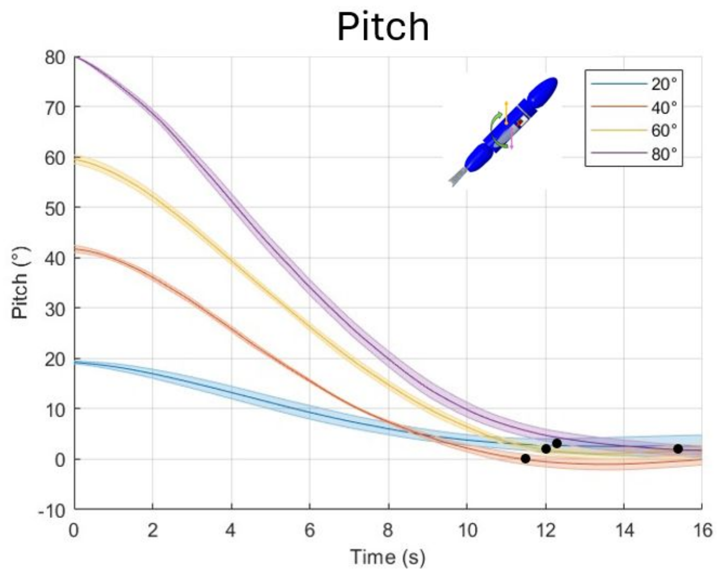

Figure 17. Pitch stability time response plot for 20°, 40°, 60°, and 80°. The black dot on each line represents the settling time.

Table 3. Mean angular velocity during the first second of each trial for fore flipper streamlined and extended configurations at 20°, 40°, 60°, and 80° pitch angles from equilibrium.

Mean angular velocity				
Fore Flipper Configuration	20° *(°/s)*	40° *(°/s)*	60° *(°/s)*	80° *(°/s)*
Streamline	0.86	1.89	2.68	4.84

Table 4. Mean standard error for fore flipper streamlined and extended configurations at 20°, 40°, 60°, and 80° pitch from equilibrium.

	Mean standard error			
Fore Flipper Configuration	20° *(±°)*	40° *(±°)*	60° *(±°)*	80° *(±°)*
Streamline	1.26	0.66	0.82	1.20

The results demonstrated that SEAMOUR's roll response resembled an underdamped system, while its pitch acted more like a critically damped system. This response was consistent with the smaller moment of inertia about the roll axis and the reduced drag encountered in that direction. As roll maneuvers will not be explored in these studies, a higher static roll stability will help isolate the effects of control surfaces on pitch and yaw maneuvers. Additionally, the low static pitch stability ensured that pitch maneuvers remain largely unaffected, allowing for a clearer evaluation of rectilinear swimming performance in terms of both thrust and lift without significant counteracting effects from hydrostatic forces.

The evaluation of SEAMOUR's passive roll and pitch stability established a critical baseline for understanding its inherent static stability, which must be assessed before investigating the system's maneuvering abilities, particularly when modifications are made to its CoG and CoB. This baseline served as a reference for assessing how static stability influenced the system's performance during dynamic tests. Specifically, these investigations help determine whether stability enhances or constrains the effectiveness of the control surfaces. This distinction is key to the subsequent discussion on the system's maneuvering capabilities and the role of static stability in shaping overall performance.

3.4. Straight Line Swimming

When a biologically derived characteristic stroke was implemented on SEAMOUR it was not able to produce straight line swimming, evident by significant pitching and heave translation. Over the course of four strokes, the system pitched up by a total of 36°, with an average of 23°. This stroke also saw heave translation of 0.38m (±0.03 m) and surge translation of 2.89 m (±0.08m) (Figure 18). The observed pitching resulted from the lift forces generated in combination with the CoG location, due to a moment arm. This shows that pitch stability can be particularly critical during propulsive strokes. Since SEAMOUR's static pitch stability is low, this stroke easily overpowered it. As the system continued pitching upward, increased surface area was exposed to the forward flow, further exacerbating pitching in subsequent strokes.

The performance of the biologically derived stroke on SEAMOUR highlighted both the stroke's limitations in straight swimming and its potential for maneuverability. Due to key differences between SEAMOUR and a biological animal, the stroke did not achieve effective straight swimming. However, it demonstrated how fore flipper lift forces generate pitching moments, which may be useful for maneuvers. Fortunately, the fore flippers are not restricted to a single set of kinematics, allowing their trajectories to be modified or additional control surfaces to be incorporated during the stroke to achieve straight swimming.

To minimize pitching and heave translation during the characteristic stroke, the pelvic section was used during the stroke, resulting in better surge translation and less overall pitching. This stroke maintained an average pitch angle of 9° and reduced the final pitch angle by 63% after four strokes, compared to trials without pelvic actuation (Figure 18). The system achieved a final horizontal translation of 3.24m (±0.09 m) and a vertical translation of -0.05m (±0.04m). These results highlight how the coordinated use of additional control surfaces during a fore flipper propulsive stroke can balance forces and produce straight swimming.

The modified side paddle stroke had the least amount of pitching and comparable surge translation as the characteristics stroke with the pelvic actuation. This stroke saw horizontal translation of 3.23 m (±0.08 m) while maintaining an average pitch angle of 2° over four strokes (Figure 18). An increase in pitch angle between seven and twelve seconds was observed, potentially due to drag from the surface antenna. Slight negative buoyancy was evident, as indicated by minimal pitching during the first three strokes while maintaining a consistent downward trend in the Z direction, resulting in a final vertical translation of -0.16 m (±0.06 m). This approach demonstrates how modifying the 3D kinematics of the fore flipper can achieve effective straight swimming, and by eliminating the need for additional control surfaces during fore flipper propulsion, these surfaces can be reallocated for coordinated maneuvers.

Low standard errors were observed in position and orientation data during various swimming and maneuvering trials. As the system swam unconstrained for 12 seconds, covering 3 meters of horizontal translation, the standard error for both horizontal and vertical displacement remained below 8% of SEAMOUR's total length. During these trials the standard error for the pitch angle was 1.5° for the characteristic stroke, 0.8° for the characteristic stroke with pelvic actuation, and 2.2° for the modified paddle stroke. These low error margins demonstrate the system's ability to have repeatable swimming performance across different gaits and configurations.

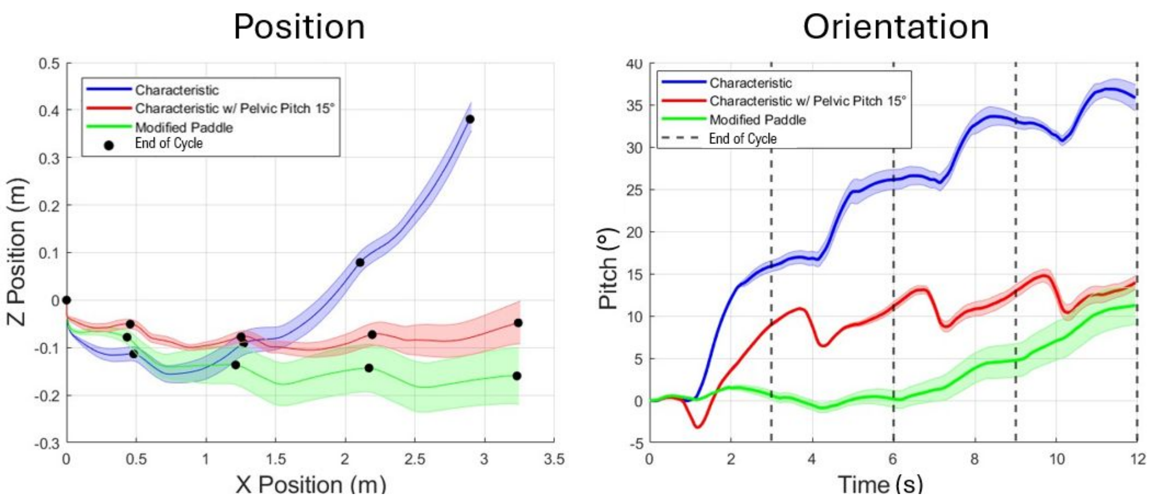

Figure 18. (Left) Position plot for three different stoke types. (Right) Pitch angle for three different stoke types.

3.5. Yaw and Pitch Turns

These experiments evaluate the system's ability to generate distinct and repeatable 3D trajectories by characterizing the sensitivity of turning performance to specific joint inputs. By recording body orientation and calculating angular rates across a range of actuation angles, these tests demonstrate the platform's consistency and repeatability—critical metrics for its validation as a research tool. While a comprehensive parametric sweep of actuation angles is detailed in a separate manuscript currently under review [REF], the results presented here highlight the fundamental performance trends and the reliability of the system under different maneuvering conditions.

During pitch maneuvers, simultaneously actuating the head and pelvis at higher angles yielded greater mean rotational rates and final angular positions, with the pelvis contributing more significantly than the head (Table 5). Comparing final angular positions, the pelvic section outperformed the head section significantly ($F(2,6)=567.52$, $p<0.001$), with a 400% increase for the 30° actuation angle and a 622% increase for the 60° actuation angle. Increasing the actuation angle from 30° to 60° had a similar impact on pelvic and combined section, with increases of 85% and 83%, respectively, while the head only had a 28% increase. When the head and pelvic sections were actuated simultaneously, the resulting angular positions closely aligned with those of the pelvic section alone, with modest 6% increase at the 30° pose angle and 5% increase at the 60° pose angle. When the head and pelvic sections were actuated simultaneously, the resulting angular positions closely aligned with those of the pelvic section alone, with no statistically significant difference observed between pelvic-only and combined actuation for either 30° ($p=0.329$) or 60° ($p=0.554$) pitch.

For yaw maneuvers, the pelvic section consistently outperformed the head section when actuated independently, while the combination of both produced the highest final angular positions ($F(2,6)=14.08$, $p=0.005$ for 60°). Comparing final angular positions, the pelvic section achieved a 129% increase over the head section for the 30° actuation angle and a 500% increase for the 60° actuation angle. When the head and pelvic sections were actuated simultaneously, the combined effect exceeded the performance of the pelvic section alone, with a 50% increase ($p=0.014$) at the 30° actuation angle and a 14% increase at the 60° actuation angle. Increasing the actuation angle from 30° to 60° had varying results depending on the section: the head section saw a -14% increase, while the pelvic section, and the combined sections exhibited increases of 118% and 67%, respectively. In the yaw studies, the head had a greater impact when the two sections were combined. This could be attributed to the hind flippers' position during the maneuver. Since they were rolled flat in these tests, they cut through the water, reducing the pelvic section's effectiveness and allowing the head's motion to exert a relatively greater influence on the generated forces.

When comparing pitch and yaw maneuvers, pitch consistently outperformed yaw in both final angular position and average turning rates ($p < 0.001$ for all configurations)(Figure 19) (Table 5). Head articulation at 30° and 60° resulted in low final angular positions, with 7° and 9° for pitch and 7° and 6° for yaw. In contrast, pelvic articulation for pitch demonstrated a significant increase in performance, with a 119% and 86% improvement over yaw at 30° and 60°, respectively. When the head and pelvis were actuated together, pitch maneuvers exhibited a 54% increase for 30° and a 70% increase for 60° compared to yaw ($t(4)=63.07$, $p<0.001$). Average turning rates for head articulation in pitch and yaw were closely aligned; however, pelvic articulation at 30° resulted in a 51% increase in pitch over yaw and a 71% increase at 60°. When combining the head and pelvis, pitch maneuvers showed a 116% increase at 30° and an 87% increase at 60° compared to yaw. Detailed values for mean turning rates are presented in Table 5.

Clear trends were evident across both pitch and yaw studies, depending on which sections were actuated. During all maneuvers, the pelvic section consistently outperformed the head, likely due to the axisymmetric shape of the head and the inclusion of large, flat hind flippers on the pelvic section, which additionally enhance its effectiveness during pitch maneuvers. For both 30° and 60° maneuvers, the pelvic section alone initially outperformed the combined actuation of the head and pelvis. In the first 0.5 seconds, the pelvic section achieved a larger initial angular change compared to the more gradual response of the combined actuation. This trend was observed in both pitch and yaw studies, with a more pronounced effect during yaw tests. This pattern becomes clearer when considering the results of head actuation alone, which consistently produced an initial negative angular position in both pitch and yaw maneuvers before transitioning to a positive angle. During head actuation, the motor, located anterior to the system's CoG, imparts a reaction moment. Consequently, the main body, containing the IMU, experiences an initial negative angular displacement. This effect can be seen most dramatically in the head pitch and yaw 60° trials. In contrast, pelvic section actuation induces the opposite effect, which can be seen most prominently in the pelvic 60° yaw plot. Unlike the yaw studies, which show a relatively linear increase, the pitch studies are influenced by restorative forces resulting from the offset between the CoG and CoB.

The findings revealed low standard errors across trials and configurations, demonstrating consistent trends. Since standard error propagated over the length of the trials, examining the error at the final 3 seconds provided insight into overall performance. At 3 seconds, the final pitch error was ±2.0° and ±0.9° for head-alone trials at 30° and 60°, respectively, ±0.4° and ±0.3° for pelvis-alone trials, and ±0.3° and ±0.4° when the head and pelvis were used together. For yaw tests, the final error for head-alone trials was ±2.4° and ±2.0°, for pelvis-alone trials was ±2.5° and ±3.1°, and for combined actuation was ±3.7° and ±0.8° at actuation angles of 30° and 60°, respectively. These results indicate that the system maintained a low error range, varying from as little as ±0.3° to a maximum of ±3.7° over the three-second turning period as it maneuvered through 3D space, demonstrating the system's repeatable performance (**Error! Reference source not found.**). To further quantify the reliability of the research platform, 95% confidence intervals (CI) were calculated for the final angular magnitudes. The system maintained a high degree of precision, with 95% CIs for primary maneuvers—such as the 60° pelvic pitch—bounded within ±6.76° of the mean (Table 5). Even at lower actuation angles, such as the 30° pelvic yaw, the 95% CI remained tight at [2.97°, 7.31°].

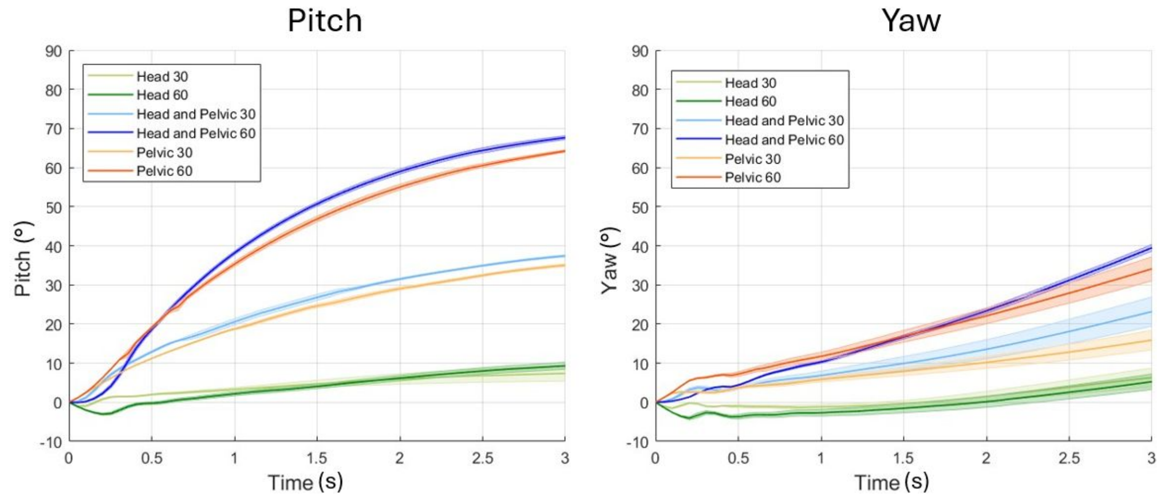

Figure 19. Pitch and yaw orientation plots for head, pelvis, and combined head/pelvis actuation for pitch and yaw turns.

Table 5. Mean turning rate for pitch and yaw trials over the 3 s trials.

Mean Turning Rates

Actuation	Pitch (°/s)	Pitch 95% CI (°)	Yaw (°/s)	Yaw 95% CI (°)
Head 30	3.17	[-0.92, 18.23]	4.12	[-6.58, 14.91]
Head 60	5.23	[7.22, 19.02]	5.33	[2.15, 10.87]
Pelvic 30	12.69	[34.65, 39.49]	8.38	[2.97, 7.31]
Pelvic 60	22.99	[60.49, 74.01]	13.45	[4.40, 23.79]
Head and Pelvic 30	11.88	[33.75, 43.11]	5.51	[5.64, 12.71]
Head and Pelvic 60	21.77	[64.29, 72.59]	11.67	[13.61, 21.96]

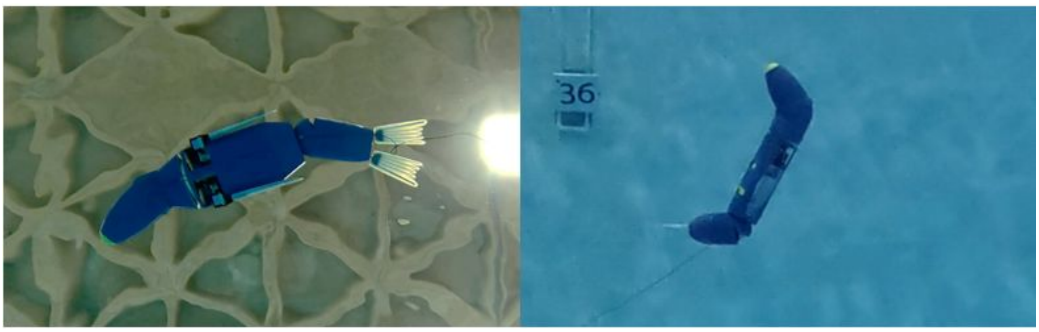

Figure 20. (Left) Head and pelvis articulated 30° during yaw test at t=3 s. (Right) Head and pelvis articulated to 60° during pitch test at t=3 s.

The initial validation trials presented here allow for a quantitative comparison between SEAMOUR's maneuvering capabilities and those of various traditional and bio-inspired UUVs (Table 6). While this study does not represent the peak performance of the system, it establishes a current benchmark for unpowered, multi-body articulation in both pitch and yaw axes. SEAMOUR's turning rate of 23°/s is comparable to established platforms like the BlueROV2/AUH and the bio-enhanced Morpheus, despite using a passive, unpowered maneuvering strategy. It is important to note that more extensive turning studies, specifically the complex interactions between the head, pelvis, and fore flippers, is explored in significantly greater depth in a follow-up study currently under review [REF]. This foundational benchmark confirms that SEAMOUR's bio-inspired architecture provides competitive maneuvering performance, which serves as a baseline for the more advanced, multi-fin coordination strategies investigated in subsequent research.

Table 6. Bio-inspired and traditional UUV turning metrics

Platform Type	System	Length (m)	Turning Radius (R/BL)	Turning Rate (°/s)	Maneuvering Strategy	Reference
Bio-inspired sea lion	SEAMOUR	1.3	0-	25	Unpowered- Head and pelvis articulation	-
California sea lion	-	1.8	0.16	660	Body bending	[18]
Bio-inspired sea lion	RSL	2.5	0.84	1.45	Powered- Head articulation	[44]
Traditional AUV	MUN Explorer	4.5	5	N/A	Traditional control surfaces	[20]
Open-Frame/ Streamline	BlueROV2/ AUH	1.0	0	20	Multiple thrusters	[45], [46]
Glider	ROUGHIE	1.3	2.3	N/A	Roll Turn w/ rear wing	[47]
Bio-enhanced Torpedo	Morpheus	0.9	1.67	25	Traditional control surfaces	[48]
Bio-robotic Fish	SAMUNO	0.6	0.2	116	Body undulation	[49]
Bio-robotic Fish	Robot D	0.4	0.53	32	Tail rudder	[50]
Bio-robotic Dolphin	robotic dolphin	1.0	0.58	13	Multi-bodied control surface	[51]

4. Conclusion and Future Work

A bio-robotic underwater system, inspired by the California sea lion, was successfully developed and validated as a capable and reliable research platform. Through a series of comprehensive swimming and maneuvering experiments, this paper has demonstrated the system's foundational design and its effectiveness as a research tool. These tests showcased the platform's versatility and repeatability, supported by a modular design built for expanding hypotheses. Beyond exploring biologically derived swimming gaits, the platform can also be tuned to investigate diverse hand-tuned or reinforcement-learned gaits. During these tests, the system demonstrated high precision, maintaining standard errors below 8% of the vehicle's total length for horizontal and vertical displacement, and exhibiting minimal angular variance, with pitch errors remaining under 2.2° across all tested swimming gaits. The system also uniquely facilitates both independent and combined evaluations of various factors contributing to its performance, as demonstrated in the yaw and pitch turns using the head and pelvis. During these turning trials, the system maintained tight orientational control, with standard errors ranging from just ±0.3° to a maximum of ±3.7° over the turning periods. Ultimately, SEAMOUR stands as a versatile and reliable platform specifically designed to advance the exploration of morphological and kinematic traits contributing to effective underwater swimming and maneuvering. By successfully translating the 3D flipper kinematics and segmented body articulation of the California sea lion into a functional robotic system, this work provides a framework for evaluating how specific biological features can be used to enhance the maneuverability of underwater vehicles.

By combining experimental testing approaches with numerical testing approaches, a better understanding of the system's capabilities can be achieved. Using SEAMOUR's computational numerical model [40], [52] allows for the examination of the system's maneuverability, exploration of new strategies for propulsion, and assessment of design modifications prior to implementation on SEAMOUR. Future tests will combine both approaches to fully assess the system's performance [REF].

While the system achieved a maximum velocity of 0.31 m/s during the swimming trials, SEAMOUR's modular design allows for modifications that can increase swimming speed. Several approaches can be explored, such as developing swimming gaits specifically tailored to the robotic platform, designing flippers with larger surface area, and replacing the current motors with models offering higher speed and torque capabilities. Additionally, incorporating supplementary control surfaces to assist with propulsion could further increase the system's velocity. Future work will investigate modifications to optimize the platform's swimming performance for a broader range of experimental applications.

Active buoyancy control should be integrated into the system's design to enable tests that isolate experimental factors and yield more repeatable results. During the current testing, constant buoyancy changes presented challenges. This was primarily due to the fact that many components were fabricated using FDM 3D printing, which experienced gradual water saturation, leading to a shift toward negative buoyancy over time. To compensate, slight adjustments were manually made to the main body's buoyancy using foam throughout the studies. Future enhancements should incorporate an active buoyancy management system, which would either maintain consistent buoyancy during operation or enable lateral buoyancy control for pitching the system.

Despite the platform's demonstrated performance, several limitations remain to be addressed in future work. While SEAMOUR's articulation is currently consolidated at the head and pelvic joints, preliminary computational modeling suggests that incorporating an additional mid-body degrees of freedom could significantly enhance turning performance. Future iterations of the engineered platform will investigate this expanded kinematic complexity. Additionally, SEAMOUR operates as a flooded system, which introduces internal fluid-structure interactions as water moves through the chassis. While design measures were implemented to mitigate these effects, further structural modifications are required to fully isolate these internal dynamics. Finally, the use of a tethered surface antenna for continuous communication during trials introduced parasitic drag. While this setup was necessary for data telemetry, the additional drag likely influenced the system's dynamics and may account for a portion of the observed variance swimming and turning trials.

For a better visualization of the swimming and maneuvering of the animal, as well as the swimming and turning trials with SEAMOUR, please see the attached supplementary video.

Acknowledgments

This research was funded by the Office of Naval Research (Dr. Tom McKenna, Program Officer, Office of Naval Research, Code 341). The funder played no role in study design, data collection, analysis and interpretation of data, or the writing of this manuscript.

The authors would like to thank Sophia P. Sebo for the work conducted in the Liquid Life Lab at West Chester University. The authors would also like to thank Anthony Paul Bibeck and Ahmet Yalim Kiral for their contributions in conducting bio-robotic experiments and collecting valuable data.

Data Availability

The raw datasets generated and/or analyzed during the current study are not publicly available but are available from the corresponding author on reasonable request.

Code availability

The underlying code for this study is not publicly available but may be made available to qualified researchers on reasonable request from the corresponding author.

Author Contributions

N.M designed and developed the robotic system. N.M., S.K., and A.D. conducted studies with the robotic system. F.E.F provided biological insights to the California sea lion. M.C.L. provided information on the fluid dynamic interaction of the fore flippers. H.G.K and J.L.T advised the project. All authors read and approved the final manuscript.

Competing Interests

The authors declare no competing interests.

Additional information

Correspondence and requests for materials should be addressed to Nicholas Marcouiller (nm875@drexel.edu).

Appendix

Main Body

The outer shell of the main body was constructed of multiple vacuum-formed sections made from 1.5 mm high-impact polystyrene (HIPS), which magnetically attach to internal support ribs for easy access to the underlying hardware. The front and rear shell sections taper smoothly from the circular head and pelvic regions to the oval-shaped central section. An aluminium U-channel serves as the structural core, providing rigidity and mounting points for internal components.

This waterproof electronics box was fabricated using a FDM 3D printer and coated with multiple layers of polyurethane to ensure waterproofing. The top opening was sealed with a 6 mm thick laser-cut acrylic sheet and a continuous 6 mm square neoprene gasket, fitted into a shallow groove to create a knife-edge seal. The lid was fastened with 4 mm bolts that connected to heat-set threaded inserts embedded from opposite side to prevent pullout. Antenna and servo motor wires were epoxy-potted into the box's sides, securely sealing all penetrations

Power and Control

Power for the system was supplied by a battery and distributed through two voltage regulators: one dedicated to the RPI and another for the motors. A 2250 mAh 3-cell LiPo battery (MaxAmps, USA) provided a minimum of two hours of continuous operation. The battery was potted in epoxy resin and fitted with waterproof connectors on both the power and balance leads, allowing it to be slid into the anterior section of the U-channel core. Power from the battery supplied a 5V 3.2A regulator (D36V28F5, Pololu, USA) for the RPI and a 15A regulator (D24V150F9, Pololu, USA) for the 14 servos (Figure 21). The servo power regulator was modified to allow it to be powered on and off via commands from the RPI, while the motor regulator was modified to operate at 8.4V, enabling each motor to reach its maximum performance of 8.2 Nm of torque and rotational speeds of 428 degrees per second.

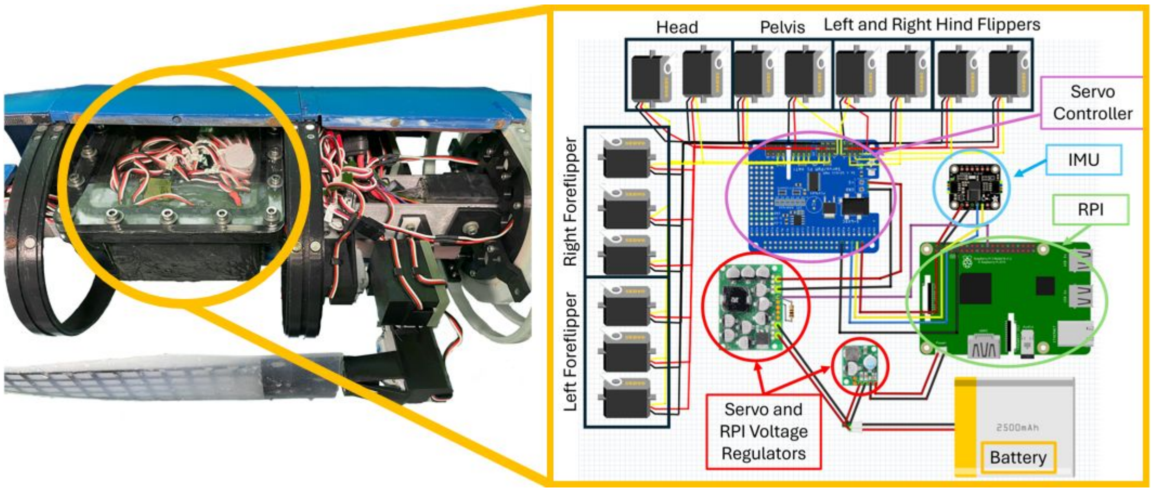

Figure 21. Location of waterproof box for electronics and schematic of electronics housed inside box.

Flipper Casting

First, a positive mold was created using an FDM 3D printer (F120, Stratasys, Minnesota USA). This mold was then vacuum-formed (450DT, Formech, USA) with clear 1.5 mm PETG sheets to produce the two halves of a negative mold. The 3D-printed support structures were positioned using a square mounting rod, which later served as the connection point to the motor assembly. The clear molds were fitted with a neoprene rubber gasket and secured using a 3D-printed framing clamp and bolts. After positioning the gridded support structure and pouring in the silicone, the molds were placed in a vacuum chamber and pulled to -25 inHg to remove any air bubbles introduced during the process. The transparent molds allowed for visual confirmation that no air pockets were present in the silicone and that the support structure was properly aligned (Figure 22).

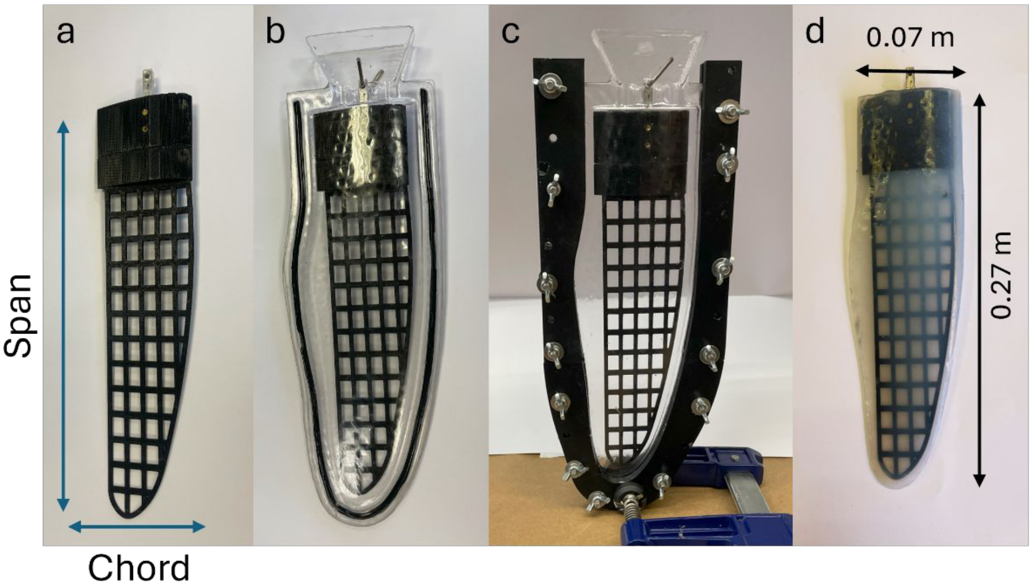

Figure 22. Flipper casting process depicted using fore flippers. Left to right: FDM 3D printed ABS support structure, support structure mounted in casting mold, mold assembled for casting, casted fore flipper

References

[1] "ONR Technology and Research," Office of Naval Research. Accessed: Feb. 25, 2025. [Online]. Available: https://p74l1103a01.dc3n.navy.mil/our-research/onr-technology-and-research
[2] "New Blue Economy | National Oceanic and Atmospheric Administration." Accessed: Feb. 25, 2025. [Online]. Available: https://www.noaa.gov/blue-economy
[3] R. Thandiackal and G. V. Lauder, "How zebrafish turn: analysis of pressure force dynamics and mechanical work," *Journal of Experimental Biology*, vol. 223, no. 16, p. jeb223230, Aug. 2020, doi: 10.1242/jeb.223230.
[4] F. E. Fish and J. T. Beneski, "Evolution and Bio-Inspired Design: Natural Limitations," in *Biologically Inspired Design: Computational Methods and Tools*, A. K. Goel, D. A. McAdams, and R. B. Stone, Eds., London: Springer, 2014, pp. 287–312. doi: 10.1007/978-1-4471-5248-4_12.
[5] P. R. Bandyopadhyay, "Trends in biorobotic autonomous undersea vehicles," *IEEE Journal of Oceanic Engineering*, vol. 30, no. 1, pp. 109–139, Jan. 2005, doi: 10.1109/JOE.2005.843748.
[6] F. E. Fish and G. V. Lauder, "Control surfaces of aquatic vertebrates: active and passive design and function," *Journal of Experimental Biology*, vol. 220, no. 23, pp. 4351–4363, Dec. 2017, doi: 10.1242/jeb.149617.
[7] G. Li, G. Liu, D. Leng, X. Fang, G. Li, and W. Wang, "Underwater undulating propulsion biomimetic robots: a review," *Biomimetics*, vol. 8, no. 3, Art. no. 3, Jul. 2023, doi: 10.3390/biomimetics8030318.
[8] P. R. Bandyopadhyay, "Guest Editorial: Biology-Inspired Science and Technology for Autonomous Underwater Vehicles," *IEEE Journal of Oceanic Engineering*, vol. 29, no. 3, pp. 542–546, Jul. 2004, doi: 10.1109/JOE.2004.833099.
[9] R. Salazar, V. Fuentes, and A. Abdelkefi, "Classification of biological and bioinspired aquatic systems: A review," *Ocean Engineering*, vol. 148, pp. 75–114, Jan. 2018, doi: 10.1016/j.oceaneng.2017.11.012.
[10] A. Wm. English, "Limb movements and locomotor function in the California sea lion (Zalophus californianus)," *Journal of Zoology*, vol. 178, no. 3, pp. 341–364, 1976, doi: 10.1111/j.1469-7998.1976.tb02274.x.
[11] S. D. Feldkamp, "Swimming in the California sea lion: morphometrics, drag and energetics," *Journal of Experimental Biology*, vol. 131, no. 1, pp. 117–135, Sep. 1987, doi: 10.1242/jeb.131.1.117.

[12] S. D. Feldkamp, “Foreflipper propulsion in the California sea lion, Zalophus californianus,” *Journal of Zoology*, vol. 212, no. 1, pp. 43–57, 1987, doi: 10.1111/j.1469-7998.1987.tb05113.x.
[13] C. Friedman and M. C. Leftwich, “The kinematics of the California sea lion foreflipper during forward swimming,” *Bioinspir Biomim*, vol. 9, no. 4, p. 046010, Nov. 2014, doi: 10.1088/1748-3182/9/4/046010.
[14] S. D. Feldkamp, R. L. DeLong, and G. A. Antonelis, “Diving patterns of California sea lions, Zalophus californianus,” *Can. J. Zool.*, vol. 67, no. 4, pp. 872–883, Apr. 1989, doi: 10.1139/z89-129.
[15] F. E. Fish, “Speed,” in *Encyclopedia of Marine Mammals*, W.F. Perrin, B. Wursig, and J.G.M. Thewissen., Academic Press, San Diego, 2002, pp. 1161–1163.
[16] D. K. Odell, “California sea lion Zalophus californianus,” in *Handbook of Marine Mammals*, S.H. Ridgway and R. Harrison., vol. 1, Academic Press. London, 1981, pp. 67–97.
[17] S. Godfrey, “Additional observations of subaqueous locomotion in the California Sea Lion (Zalophus californianus),” *Aquatic Mammals*, vol. 11, no. 2, pp. 53–57, 1985.
[18] F. E. Fish, J. Hurley, and D. P. Costa, “Maneuverability by the sea lion Zalophus californianus: turning performance of an unstable body design,” *Journal of Experimental Biology*, vol. 206, no. 4, pp. 667–674, 2003, doi: 10.1242/jeb.00144.
[19] N. M. Puzai, A. F. Ayob, and M. R. Arshad, “A review on recent advancements in unmanned underwater vehicle design,” *J. Ocean, Mech. Aerospace-sci Eng.*, vol. 31, no. 1, pp. 1–8, 2016.
[20] M. T. Issac, S. Adams, M. He, N. Bose, C. D. Williams, R. Bachmayer, and T. Cress, “Manoeuvring Experiments Using the MUN Explorer AUV.” Accessed: Jan. 15, 2026. [Online]. Available: https://ieeexplore.ieee.org/document/4231121
[21] M.-G. Kim, H. Kang, M.-J. Lee, G. R. Cho, J.-H. Li, and C. Kim, “UUV platform optimal design for overcoming strong current,” *J. Ocean Eng. Technol.*, vol. 35, no. 6, pp. 434–445, Dec. 2021, doi: 10.26748/KSOE.2021.069.
[22] X. Li, D. Zhang, M. Zhao, X. Wang, and Y. Shen, “Hydrodynamic Analysis and Drag-Reduction Design of an Unmanned Underwater Vehicle Based on Computational Fluid Dynamics,” *Journal of Marine Science and Engineering*, vol. 12, no. 8, Aug. 2024, doi: 10.3390/jmse12081388.
[23] D. L. Rudnick, R. E. Davis, D. M. Fratantoni, and M. J. Perry, “Underwater Gliders for Ocean Research,” *Marine Technology Society Journal*, vol. 38, 2004, Accessed: Jan. 23, 2025. [Online]. Available: https://www.researchgate.net/publication/233687927_Underwater_Gliders_for_Ocean_Research
[24] A. Bender, D. Steinberg, A. Friedman, and S. Williams, “Analysis of an autonomous underwater glider,” *Australasian Conference on Robotics and Automation*, pp. 1–10, Jan. 2008.
[25] D. C. Webb, P. J. Simonetti, and C. P. Jones, “SLOCUM: an underwater glider propelled by environmental energy,” *IEEE Journal of Oceanic Engineering*, vol. 26, no. 4, pp. 447–452, Oct. 2001, doi: 10.1109/48.972077.
[26] F. E. Fish, “Advantages of aquatic animals as models for bio-inspired drones over present AUV technology,” *Bioinspir. Biomim.*, vol. 15, no. 2, p. 025001, Feb. 2020, doi: 10.1088/1748-3190/ab5a34.
[27] A. P. Mignano, S. Kadapa, A. C. Drago, G. V. Lauder, H. G. Kwatny, and J. L. Tangorra, “Fish robotics: multi-fin propulsion and the coupling of fin phase, spacing, and compliance,” *Bioinspir. Biomim.*, vol. 19, no. 2, p. 026006, Jan. 2024, doi: 10.1088/1748-3190/ad1dba.
[28] A. P. Mignano, S. Kadapa, J. L. Tangorra, and G. V. Lauder, “Passing the Wake: Using Multiple Fins to Shape Forces for Swimming,” *Biomimetics*, vol. 4, no. 1, 2019, doi: 10.3390/biomimetics4010023.
[29] C. H. White, G. V. Lauder, and H. Bart-Smith, “Tunabot Flex: a tuna-inspired robot with body flexibility improves high-performance swimming,” *Bioinspir. Biomim.*, vol. 16, no. 2, p. 026019, Mar. 2021, doi: 10.1088/1748-3190/abb86d.
[30] R. Baines, S. K. Patiballa, J. Booth, L. Ramirez, T. Sipple, A. Garcia, F. Fish, and R. Kramer-Bottiglio, “Multi-environment robotic transitions through adaptive morphogenesis,” *Nature*, vol. 610, no. 7931, pp. 283–289, Oct. 2022, doi: 10.1038/s41586-022-05188-w.
[31] Z. Chen, T. I. Um, J. Zhu, and H. Bart-Smith, “Bio-Inspired Robotic Cownose Ray Propelled by Electroactive Polymer Pectoral Fin,” in *Volume 2: Biomedical and Biotechnology Engineering; Nanoengineering for Medicine and Biology*, Denver, Colorado, USA: ASMEDC, Jan. 2011, pp. 817–824. doi: 10.1115/IMECE2011-64174.
[32] P. Liljebäck and R. Mills, “Eelume: A flexible and subsea resident IMR vehicle,” in *OCEANS 2017 - Aberdeen*, Jun. 2017, pp. 1–4. doi: 10.1109/OCEANSE.2017.8084826.

[33] E. Kelasidi, P. Liljeback, K. Y. Pettersen, and J. T. Gravdahl, “Innovation in Underwater Robots: Biologically Inspired Swimming Snake Robots,” *IEEE Robotics & Automation Magazine*, vol. 23, no. 1, pp. 44–62, Mar. 2016, doi: 10.1109/MRA.2015.2506121.
[34] S. Randeni, E. M. Mellin, M. Sacarny, S. Cheung, M. Benjamin, and M. Triantafyllou, “Bioinspired morphing fins to provide optimal maneuverability, stability, and response to turbulence in rigid hull AUVs,” *Bioinspir. Biomim.*, vol. 17, no. 3, p. 036012, Apr. 2022, doi: 10.1088/1748-3190/ac5a3d.
[35] Y. Wang, Y. Guo, S. Yang, T. Sun, X. Wang, and H. Zhou, “Design, Hydrodynamic Analysis, and Testing of a Bio-inspired Movable Bow Mechanism for the Hybrid-driven Underwater Glider,” *J Bionic Eng*, vol. 20, no. 4, pp. 1493–1513, Jul. 2023, doi: 10.1007/s42235-023-00361-x.
[36] A. M. Leahy, F. E. Fish, S. J. Kerr, J. A. Zeligs, S. Skrovan, K. L. Cardenas, and M. C. Leftwich, “The role of California sea lion (Zalophus californianus) hindflippers as aquatic control surfaces for maneuverability,” *J Exp Biol*, vol. 224, no. 20, p. jeb243020, Oct. 2021, doi: 10.1242/jeb.243020.
[37] S. J. Kerr, F. E. Fish, A. J. Nicastro, J. A. Zeligs, S. Skrovan, and M. C. Leftwich, “Biomechanical energetics of terrestrial locomotion in California sea lions (Zalophus californianus),” *Journal of Experimental Biology*, vol. 225, no. 18, p. jeb244163, Sep. 2022, doi: 10.1242/jeb.244163.
[38] G. Perrotta, F. E. Fish, D. S. Adams, A. M. Leahy, A. M. Downs, and M. C. Leftwich, “Velocity Field Measurements of the California Sea Lion Propulsive Stroke Using Bubble PIV,” *Fluids*, vol. 7, no. 1, Art. no. 1, Jan. 2022, doi: 10.3390/fluids7010003.
[39] J. Wu, S. Xu, H. Liao, C. Ma, X. Yang, H. Wang, T. Zhang, and X. Han, “Maneuverability and Hydrodynamics of a Tethered Underwater Robot Based on Mixing Grid Technique,” *Journal of Marine Science and Engineering*, vol. 9, no. 6, p. 561, Jun. 2021, doi: 10.3390/jmse9060561.
[40] S. Kadapa, A. Drago, N. Marcouiller, J. L. Tangorra, and H. G. Kwatny, “Development of numerical model for a bio-inspired sea lion robot,” *IEEE Journal of Oceanic Engineering*, 18 2025.
[41] P. W. Webb, “Maneuverability - general issues,” *IEEE Journal of Oceanic Engineering*, vol. 29, no. 3, pp. 547–555, Jul. 2004, doi: 10.1109/JOE.2004.833220.
[42] A. Drago, N. Marcouiller, S. Kadapa, F. E. Fish, and J. L. Tangorra, “Propulsive Force Characterization of a Bio-Robotic Sea Lion Foreflipper: A Kinematic Basis for Agile Propulsion,” *Biomimetics*, vol. 10, no. 12, Dec. 2025, doi: 10.3390/biomimetics10120831.
[43] A. Drago, S. Kadapa, N. Marcouiller, H. G. Kwatny, and J. L. Tangorra, “Using Reinforcement Learning to Develop a Novel Gait for a Bio-Robotic California Sea Lion,” *Biomimetics*, vol. 9, no. 9, p. 522, Aug. 2024, doi: 10.3390/biomimetics9090522.
[44] S. Liu, Y. Liu, Z. Zhang, H. Bai, J. Du, and B. Cao, “A flexible bionic head for improving turning maneuverability of the robotic sea lion: design, dynamics, and experiment,” *Ocean Engineering*, vol. 343, p. 123286, Jan. 2026, doi: 10.1016/j.oceaneng.2025.123286.
[45] R. D. Christ and R. L. Wernli, *The ROV Manual: A User Guide for Observation-Class Remotely Operated Vehicles*, 1st ed. Elsevier Ltd. Butterworth-Heinemann, 2007.
[46] Z. Wang, X. Liu, H. Huang, and Y. Chen, “Development of an Autonomous Underwater Helicopter with High Maneuverability,” *Applied Sciences*, vol. 9, no. 19, Art. no. 19, Jan. 2019, doi: 10.3390/app9194072.
[47] B. R. Page, S. Ziaeefard, A. J. Pinar, and N. Mahmoudian, “Highly Maneuverable Low-Cost Underwater Glider: Design and Development,” *IEEE Robotics and Automation Letters*, vol. 2, no. 1, pp. 344–349, Jan. 2017, doi: 10.1109/LRA.2016.2617206.
[48] S. Randeni, M. Sacarny, M. Benjamin, and M. Triantafyllou, “Morpheus: An A-sized AUV with morphing fins and algorithms for agile maneuvering,” 2022, doi: 10.48550/ARXIV.2212.11692.
[49] A. P. Mignano, “Understanding multi-fin swimming and maneuvering to develop highly capable swimming,” Drexel University, 2025.
[50] B. Pollard and P. Tallapragada, “Passive Appendages Improve the Maneuverability of Fishlike Robots,” *IEEE/ASME Transactions on Mechatronics*, vol. 24, no. 4, pp. 1586–1596, Aug. 2019, doi: 10.1109/TMECH.2019.2916779.
[51] Z. Yang, W. Gong, H. Chen, S. Wang, and G. Zhang, “Research on the Turning Maneuverability of a Bionic Robotic Dolphin,” *IEEE Access*, vol. 10, pp. 7368–7383, 2022, doi: 10.1109/ACCESS.2022.3142521.
[52] S. Kadapa, N. Marcouiller, A. Drago, J. L. Tangorra, and H. G. Kwatny, “Tuning hydrodynamic coefficients using a genetic algorithm for a numerical model of a bio-robotic sea lion”, Accessed: Mar.

03, 2026. [Online]. Available:
https://www.authorea.com/doi/full/10.36227/techrxiv.175825699.90870419?commit=7e1f1a57012d29218d3769ad98b13ca340a9db8b